Summer 2012

Gray gas analysis of radiative preheating effects on shock induced combustion

Pratibha Raghunandan

Department:

GRAY GAS ANALYSIS OF RADIATIVE PREHEATING EFFECTS ON SHOCK INDUCED COMBUSTION

by

PRATIBHA RAGHUNANDAN

A THESIS

Presented to the Faculty of the Graduate School of the

MISSOURI UNIVERSITY OF SCIENCE AND TECHNOLOGY

In Partial Fulfillment of the Requirements for the Degree

MASTER OF SCIENCE IN AEROSPACE ENGINEERING

2012

Approved by

Dr. Kakkattukuzhy M. Isaac, Advisor
Dr. Kelly O. Homan
Dr. James A. Drallmeier

ABSTRACT

The use of detonations in combustors has been receiving increased attention in recent times. The presence of shock waves in such combustors invariably poses the existence of two domains that present different physics for the flow processes. The variation of upstream temperature due to radiative heating by the products of combustion was given particular attention in the present study. The modeling of heat transfer across a normal shock wave of negligible thickness was done by considering the reactants and the products of combustion to be in radiative equilibrium with each other.

The quantification of emissivity of the products of combustion required the use of suitable numerical gray gas models. Similarly, experimental data from literature were used to obtain the absorptivities of the gaseous reactants used for analyses. The behavior of the species in the reactions were dependent upon the chemical kinetics mechanism used in this study, the reduced GRI-Mech 1.2 mechanism - DRM 19. Parametric analysis of the reactant mixture was carried out to analyze its effect on the upstream variation of temperature and on the absorption length. It was found that a decrease in the inertness of the reactant mixture and the addition of polyatomic gases receptive to radiation reduced the absorption lengths. Increased inlet pressures were found to have increased impact on the upstream region and resulted in extremely small increases in flow temperature. The subsequent effects of radiative preheating on ignition delay were studied and more pronounced reductions in induction times were observed with more oxygen content in the reactants. Overall, the study with one-dimensional approximation provides for an understanding of the process of detonations and describes the inter-dependence of radiative heat transfer and downstream chemical kinetics.

ACKNOWLEDGEMENTS

I wish to express my gratitude to my advisor, Dr. K. M. Isaac, for his diligent guidance while doing research. His patience and support have been very valuable during the program and I am thankful for the several lessons I have learnt along the way. I am grateful to him for providing an opportunity for me to do research on a challenging problem and for being a mentor in many ways.

I also wish to thank my committee members Dr. Kelly Homan and Dr. James Drallmeier for their valuable suggestions and timely review of my thesis. I thank Dr. Drallmeier for providing all facilities of the department for my research and for the financial assistance I received in the form of a graduate teaching assistantship. A special note of thanks to Dr. Homan for his unwavering encouragement and support in my education. It was truly comforting to be greeted with a warm smile and to engage in thoughtful, pleasant conversations with him.

Thanks to Mr. Matthew Pickens, Ms. Sherry Mahnken and Mr. Chris Jocius for assisting with locating some archival papers used for this study and for being patient in acquainting me with their very many savvy search methodologies.

Finally, I thank my family for all their love, support and encouragement.

TABLE OF CONTENTS

LIST OF ILLUSTRATIONS

LIST OF TABLES

NOMENCLATURE

Symbol	Description
ϵ	Emissivity
ϵ_T	Total emissivity of a mixture of gases
ϵ_0	Equivalent emissivity at zero partial pressure or a pressure of 1 bar
a_0	Fine structure parameter, indicative of the line density, of the interval
a_i	- Coefficient as described in equation 3
	- Temperature dependent weighting factor for emissivity as given by Hottel
λ^i	Logarithm of partial pressure-path length product ($\log pL$) corresponding to the i^{th} order polynomial
c_{ji}	Coefficient to describe total emissivity as described by Leckner [14]
τ	- Temperature (K)/1000
	- Ignition delay time (μs)
ign	Ignition (subscript)
M, N	Polynomials of second order as described in equations 2 & 3
$T(x), T(y), T(z)$	Temperatures represented by Chebychev polynomials as described by Modak [15] (K)
c_{ijk}	Coefficients for CO_2 and H_2O polynomial fits used to describe gas emissivity by Modak [15]
T	- Transmittance of gas sample
	- Temperature of gas (K)
α	- Absorption coefficient of hydrocarbon gases (cm-atm)$^{-1}$

	- Length of sample chamber used to measure transmittance of a gas (cm)
p,P	Pressure or partial pressure of gases as the case maybe (atm, MPa)
ϕ	Equivalence ratio
X	Mole fraction of gas
R, R^0	Universal gas constant (cal K^{-1} mol^{-1})
k_i	- i^{th} elementary reaction rate coefficient
	- Temperature independent absorption coefficients for a gray gas as given by Hottel
A	Pre-exponential constant
β, n	Temperature coefficient in the Arrhenius equation
E, E_A	Activation energy (kJ/mol or cal/mol)
S	Sensitivity of a reaction in a mechanism
ρ	Density
u	- Velocity
	- Internal energy per unit mass of the gas mixture
h	Enthalpy
t	time
v	Mass-averaged velocity of the gas mixture
Y_i	Mass fraction of species i
ω_i	Rate of production of species i by chemical reactions (mass per unit volume per unit time)
f_i	External force per unit mass on species i
R_{gas}	Specific gas constant
$C_{p,F}$	Species enthalpies in mass units
σ	Stefan-Boltzmann constant ($W/(m^2\text{-}K^4)$)
γ	Specific heat ratio

M	Mach number
C_P	Specific heat at constant pressure
$\dot{m}$	Mass flow rate of the gas
A	Area of cross-section
q	Heat-flux vector
q_R	Radiant heat-flux vector
V_i	Diffusion velocity of species i
λ	Thermal Conductivity
$D_{T,i}$	Thermal diffusion coefficient for species i
$D_{i,j}$	Binary diffusion coefficient for species i and j
L	Length of the emitting region
α_i, β_i	Weighting coefficients given by Coppalle et al. [48] which is used as a substitute for a_i given by Hottel
a	Absorptivity (cm^2 mol^{-1})
I_0	Intensity of total laser signal (mV)
I	Intensity of transmitted laser signal (mV)
c	Concentration of gas sample (mol cm^{-3})
b	Optical pathlength (=9.6 cm) as per the experiment conducted by Olson et al. [51]

1. INTRODUCTION

1.1. BACKGROUND AND MOTIVATION

Propulsion devices such as ramjets, pulse detonation engines, scramjets and gas turbines require detailed analyses of the combustion processes in order to enable efficient combustor designs. Fluid mechanical processes coupled with chemical kinetics modeling support the understanding of the complex phenomena associated with combustion devices of practical significance [1]. Combustion phenomena are a challenge to model mathematically as they involve several processes such as mixing, heat transfer and mechanism - dependent reactions. The advancements in computational fluid dynamics (CFD) techniques enable the simulation of such complex flows without a significant loss in accuracy.

Traditionally, deflagration has been the mode of combustion in gas turbine engines. Detonations with an inherent capability to burn fuel-oxidizer mixtures efficiently have been on the radar of researchers to harness its potential in practical combustors [2], with a renewed interest in recent times on pulsed detonations. Detonation based combustors have several advantages to offer, key among them being, simplicity in design and increased thermodynamic efficiency in comparison with the Brayton cycle used in conventional engines. Studies on mixture autoignition properties, effect of initial mixture pressure and temperature on detonations [3] and effects on reaction induction times have been considered, among several others. Despite such studies on detonation processes, their usage in practical combustors is one that is yet to be attained [4], highlighting the importance of incorporating more parametric investigations.

Several gas-dynamic and molecular-level mechanisms have been modeled to analyze the heat transfer modes in detonation waves [3]. The concept explored in these studies is one of heat transfer from detonation products to the fresh mixture.

The heat fluxes involved being large compound the complexities of the flow which is typically characterized by the presence of strong shock waves and reacting mixtures. Numerical methods would invariably provide for a lucrative option of analyses with sufficient resolution of the flow.

1.2. OBJECTIVE OF STUDY

The nonequilibrium process of energy transfer by radiation has long been studied in several contexts, especially in studies concerning astrophysical applications. The nonequilibrium process, which could be a challenge to model in itself has often been studied assuming sources such as molecular transport, dissociation and vibration have negligible effects [5]. This heat transfer process entails heat loss from the radiating region behind the shock wave. With sufficiently high temperatures downstream of a shock wave, these radiative effects would be felt upstream, a consequence of intuitive reasoning. The overall changes in temperature and heat flux from infinity upstream to infinity downstream due to the intermediate non-adiabatic processes (between computational cells) but an adiabatic process in totality (for the entire one-dimensional space under study) have been considered. Solutions to the non-linear conservation equations was the prime subject of study from the 1950s up to about three decades later, with the most significant contribution hailing from Heaslet and Baldwin [6].

Heaslet and Baldwin produced numerical solutions to continuum, inviscid flow shock wave relations with the inclusion of radiation transport equation. Their work followed on the heels of the paper by Zel'dovich [7] which presented an analytical approach to determine the presence of discontinuities in the temperature and velocity profiles. They, however, analyzed the uniqueness of the solutions and made a more comprehensive study under parametric variations. Through the introduction of dimensionless parameters to quantify the shock and radiation strengths, their study presented nonlinear variations in temperature, velocity and heat flux (Figure 1.1.).

They performed such an analysis for nine combinations of shock and radiation strengths (Figure 1.2.).

The heat flux vector due to radiation in the above cases for the gray gases took the form of an integro-differential equation which was further simplified with certain exponential approximations made to the kernel functions [8]. The integro-differential terms that got incorporated in their work was the result of the introduction of a dimensionless distance and the integration of the heat flux over this distance. The approaches, purely mathematical in nature, aimed at solving the conservation equations with simplicity and verifying the monotonicity of the non-linear temperature and velocity profiles. While the physics behind these methods essentially remained the same, the rigorous analytical approaches served an important purpose, one of depicting the rise in temperature ahead of the shock with verifiable, applicable results.

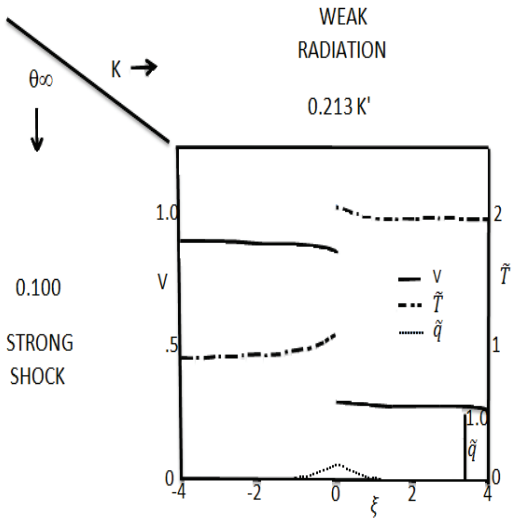

Figure 1.1. Magnified image of the variation of dimensionless velocity V, temperature $\tilde{T}$ and heat flux $\tilde{q}$ profiles obtained by Heaslet and Baldwin for the case of weak radiation and strong shock [6]. ξ signifies dimensionless distance. θ_∞ and K correspond to shock and radiation strengths as defined by Heaslet and Baldwin.

In the context of combustion, one might easily conjecture that the heat released due to sufficiently high temperatures attained could result in similar effects

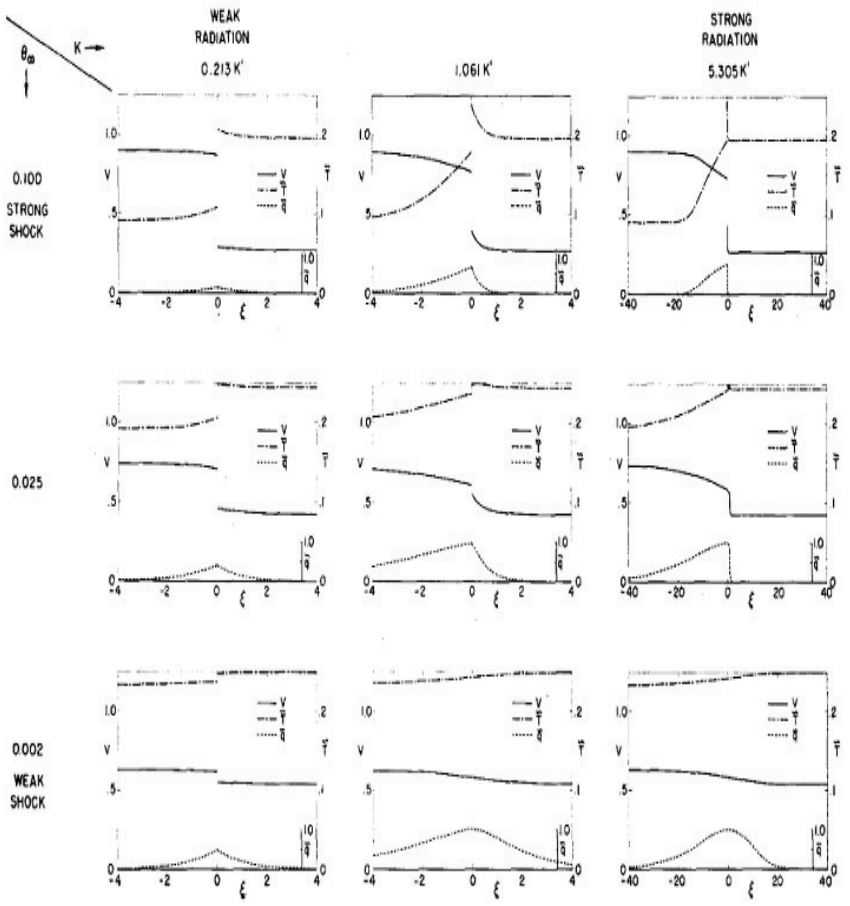

Figure 1.2. Dimensionless velocity V, temperature $\tilde{T}$ and heat flux $\tilde{q}$ profiles obtained by Heaslet and Baldwin for different shock and radiation strengths [6].

if "supported" by a shock wave. This line of thought forms the basis of the study being hereby reported. The current study focuses on the heat fluxes involved in detonations. It is of interest to quantify this radiative heat flux term and determine the implications of incorporating this term in the governing flow relations.

The present study deviates from the ones reported above by the presence of the combustion process. This leads to a modification in the flow equations and necessitates the need to investigate real properties of gases of relevance. The consequent effects on species of the reactions, ignition properties and chemical kinetics models, all in the realm of numerical studies based on Eulerian type, finite volume CFD codes shall be explored.

2. LITERATURE REVIEW

The literature review relevant to the present study has been categorized into four parts. The survey will focus on radiation studies in combustion phenomena in general, followed by modeling of relevant terms, shock wave and ignition delay studies that can most closely relate to the concepts explored in the current study.

2.1. STUDIES ON RADIATION IN COMBUSTION PHENOMENA

With the advancement in CFD techniques and computational power, much effort has been made to develop more important and comprehensive models in combustion with sufficient emphasis on the need to incorporate thermal radiation models. The importance of radiative heat transfer at the high temperatures normally attained during combustion have been emphasized in relation to domains such as industrial furnaces, combustion rate control in fires, internal combustion engines and gas turbine combustors. These radiation models developed have different approaches depending upon the details required. Studies have ranged from determination of flame structure, soot producing capabilities of flames, local radiative heat flux (including spectral studies) and temperature distribution [9]. The determination of temperature distribution is known to have particular relevance in chemical kinetics studies and thereby on the much sought for alleviation of pollutant concentrations.

The rise in studies on radiation flux quantification in gas turbine combustors in the 1970's was from the realization of penalties involved in cooling the walls of the combustor. Typically, a part of the combustor airflow was used to envelop the walls of the combustor and cool it to reduce liner deterioration. However, it was soon discovered that this voluminous film air contributed to incomplete combustion and thereby unburnt hydrocarbons during engine idling conditions. Any attempt to reduce this cooling mandated a good understanding of the radiation effects of combustion. Lefebvre [10] explained the development of studies in this aspect with regard to luminous (flames with soot particles) and non-luminous flame radiation. While these

studies may have looked at two and three dimensional geometrical aspects, they nevertheless emphasized the need to look at radiation in combustion problems which will be implemented through one-dimensional studies in the present work.

The choice of radiation models to be used for analysis in such applications would typically depend upon the desired radiation quantities. Radiation in practical applications possess spectral (dependence on frequencies) and directional (dependence on solid angle) variations. The choice of the model would result in the radiant energy equation taking on varying forms of simplicity. The details required for determination of flame structure and the effects in enclosures would be fairly intense to necessitate the need for energy balance methods such as zonal, Monte-Carlo, finite element or volume. Viskanta [11] described the use of these methods in great detail. The zonal and finite element/volume approaches involve the region of interest to be divided into zones/ elements with walls included, if necessary. The temperature, composition of species, and emissivity/transmissivity characteristics are assumed to be uniform in each of these regions [10]. The adoption of such methods implies the necessity to solve simple but computationally expensive simultaneous algebraic equations. Monte-Carlo methods on the other hand involve a similar approach in a three-dimensional space but possess a simplification in the computations due to radiative exchange being treated in a probabilistic manner.

For the determination of total heat flux requirements from the flame, the details required would be fairly simpler than in the previous cases and thus gray gas assumptions utilizing global radiation properties (particle properties integrated, twice to be more precise, over various frequencies and solid angles) would suffice for analysis. The energy conservation equation which is usually an integro-differential equation [9] would become simplified with the source term for radiation expressed as a fraction of black body radiation intensity. The non-scattering gray gas models provide for easier understanding of the processes without too many errors in the resulting equations [12].

2.2. MODELING OF VARIOUS PARAMETERS

Quantification of radiative heat flux from the flame region mandates the evaluation of radiative properties of the combustion gases. Typical products in combustors with hydrocarbon flames include but are not necessarily limited to H_2O, CO_2 and N_2 with minor species such as CO, NO, OH, O_2 and H_2 among others. Among the major species, H_2O and CO_2 are the most prominent ones and can characterize the flames to a large extent while diatomic molecules such as N_2, H_2 and O_2 have no appreciable contribution to radiation [10]. Similarly, determination of any upstream effects as described in Section 1 would require the determination of the absorption characteristics of the reactants. These characteristics have been studied to varying extents as summarized below.

2.2.1. Emissivity. Emissivity of gases is known to depend upon temperature, pressure, composition and mean beam length, a measure of size and shape of the gas volume under consideration. Hottel's charts [13] were the traditional means of determining the emissivities of the products of combustion wherein the charts depicted the variation of emissivity of water vapor and carbon dioxide with temperature and the products of the partial pressure and path length of the gases. The curves that Hottel obtained by experimental methods possessed negative slopes with extrapolated regions at higher temperatures. Thus, it was well established that emissivity had smaller magnitudes at higher temperatures and at lower pressure-path length products. Since then, the accuracy of Hottels charts and their applicability to varying operating conditions have been much debated. Inaccuracies introduced due to pressure-broadening effects of spectral lines and overlapping of CO_2 and H_2O spectral bands were recognized and modified empirical relations were proposed.

Leckner [14] presented a theoretical relationship for pressure correction and overlap correction by a comparison between various models, mathematically represented as follows.

$$\epsilon = \epsilon_{H_2O} + \epsilon_{CO_2} - \Delta\epsilon \tag{1}$$

The corrections proposed proved to be more accurate than previous studies. The total emissivity was expressed in the form of simple coefficient dependent relations.

$$ln(\epsilon_0) = a_0 + \sum_{i=1}^{M} a_i \lambda^i \tag{2}$$

where,

$$a_i = c_{0i} + \sum_{i=1}^{N} c_{ji} \tau^j \tag{3}$$

His studies were conclusive of emissivity being independent of pressure at high temperatures where the curves reached a saturation limit and that the overlap correction was negligibly small at path-lengths below 20 bar-cm. Subsequently, Modak [15] suggested a temperature variation to Leckner's overlap correction correlation and expressed total emissivity in terms of products of Chebychev polynomials.

$$ln(\epsilon) = \sum_{i=0}^{2} T_i(x) \sum_{j=0}^{3} T_j(y) \sum_{k=0}^{3} c_{ijk} T_k(z) \tag{4}$$

His model was valid below 1.0 atm and 2000 K.

Lallemant [16] made an extremely detailed study of emissivity correlations for homogenous and non-homogenous mixtures and explored their coupling to the radiative transfer equation (RTE). His compilation of emissivity studies presented the limiting ranges of total pressures, temperatures and partial pressure-path lengths that govern each model. This proves to be very useful in assessing the application of a model to desired CFD codes and in the selection of an appropriate model to the present study. Models such as the weighted sum of gray gases model (WSGGM) and hybrid models which combined the polynomial approximations of Leckner, Modak and the WSGGM were analyzed. The WSGGM put forth the total emissivity of a gas mixture as the sum of a number of gray gases, each of them being associated with

a temperature-dependent weighting coefficient. He clearly brought out the fact that WSGGMs, though more amenable to incorporation in differential-form RTEs than polynomial approximations, possess inherent inaccuracies due to their limitation to CO_2 and H_2O partial pressure values of one and two.

Emissivity studies thus have spanned over several decades with more emphasis being made on development of models that can be easily incorporated into computer codes. Experiments backing these models have been relatively limited due to the difficulties in accurate measurements of temperature. Usage of IFRF (International Flame Research Foundation) type probes for intrusive measurement of temperature through suction pyrometry has been typical of the standard experimental methods used [16]. Recent attempts in in-situ measurements have been the usage of image processing techniques to analyze images captured by color image detectors [17] but have limited applications. The dearth of experimental data to back theoretical relations at high temperatures and low pressures continues to be the drawback in this area.

2.2.2. Absorptivity. Absorptivity of gases has largely been studied with regard to the products of combustion as stated above. Often, Kirchoff's law of blackbody radiation is invoked as an approximation to determine the absorptivity of gases from their emissivity characteristics. Liu et al. [18], in a recent study, suggested ways to account for the non-gray nature of absorptivity of gases while using gray gas models. Their method involved an initial guess for the equivalent absorption coefficient and prediction of temperature profile in the gas volume. Comparisons were made with accurate non-gray solutions and any differences observed were corrected by using a conjugate-gradient method. While this innovative method is very accurate, it was restricted to CO_2 and H_2O.

For absorption characteristics of reactants as in the present study, a survey of hydrocarbon gas absorption is critical. Existent literature on absorptivity of hydrocarbon gases is largely experimental in nature. The helium-neon laser emission

line at 3.39 μm being very close to the fundamental vibration frequency of the coupling between carbon and hydrogen atoms, has been commonly used [19]. The procedure as adopted by Jaynes et al. [19] involved the evacuation of the absorption cell and later measuring the transmission of the laser beam through the hydrocarbon-air mixtures. This was performed over a range of pressures and at room temperature. The absorption coefficient, in units of $(\text{cm-atm})^{-1}$ can be computed from their data using the Beer-Lambert's law for transmittance through a gas sample. The representative relation is shown below.

$$T = e^{-\alpha p x} \tag{5}$$

Their results showed greater absorption by ethane than methane, as against low-resolution spectroscopic data by Pierson et al. [20].

The temperature dependent absorption characteristics of several hydrocarbons have been studied by Klingbeil et al. [21] with respect to higher order aliphatic hydrocarbons and a few aromatic hydrocarbons. The fixed wavelength temperature dependent measurements at 3.39 μm were compared with the Fourier transform infrared spectroscopy results and good agreements were obtained for the temperature range of 25°C - 500°C. They obtained a near-linear dependence of absorption coefficients on temperature at various frequencies of the laser. However, this dependence of absorption on temperature was found to be valid for smaller hydrocarbons such as methane and ethylene as pointed out in another set of studies involving a 3.39μm laser [22]. Cross sections of larger hydrocarbons were found to be independent of the pressure or temperature of the gas sample and the results proved applicabilities to pulse detonation engines due to the wide operating ranges used. The choice of the laser line strength used to determine the absorption characteristics depends upon the peak absorption bands of the hydrocarbons used. While 3.39μm corresponds to the fundamental vibration between C-H atoms, absorption spectra near 1.646 μm have also been determined. However, these have been limited to CH_4 and C_3H_8 [23].

Measurements of molar extinction coefficients using shock tube techniques were made to obtain a database for temperature measurements [24]. The extinction coefficients could be directly related to absorption of the unburnt hydrocarbon gases (aliphatic and aromatic). In this study by Tsuboi et al., of the various mixtures tested, methane and ethane were the only hydrocarbons to exhibit reduction in the extinction coefficient with increasing density and temperature. The reduction was attributed to pressure-broadening[1] and Doppler-broadening[2] effects. While the results of such studies involving fairly complex analysis could have implications for non-gray gas models, the analyses by themselves are inconsequential to gray gases.

The various experimental efforts however provide values for absorptivity or similar parameters (depending upon the model) which can be easily used to determine the absorption coefficient by applying the Beer-Lambert's law as described above.

2.3. SHOCK INDUCED COMBUSTION

2.3.1. Theoretical Studies. Shock waves have been studied in a variety of contexts including the Chapman-Jouguet (CJ) and Zel'dovich, von Neumann and Döring (ZND) theories. Razani [25] carried out one such survey wherein he described detonation waves to be composed of a lead shock wave responsible for the initiation of chemical reaction. The survey covered mathematical criteria for the stability of detonation waves of varying strengths using the above theories. The CJ velocity represents the minimum sustainable velocity for the detonation and represents the speed where the burnt gas is sonic relative to the shock wave. Typically, detonations are overdriven with the detonation wave travelling at speeds greater than the CJ velocity.

[1]Pressure-broadening is the process by which the band-width increases due to increased collisions between molecules at high pressures.

[2]Doppler broadening is the line broadening due to an increase in frequency of incoming radiation from the molecules' perspective. Higher velocity of molecules upon absorption of radiation is known to be the cause of this.

From a Rankine-Hugoniot analysis, such overdriven detonations possess two possible solutions, strong detonations corresponding to the subsonic branch on the Hugoniot curve and weak detonations corresponding to the supersonic branch on the curve [26]. These "strong" or "weak" detonations need a quantitative benchmark in the present study. The most commonly used methods in literature date back to the seminal work by Clarke [27] who attempted this quantification in radiative shocks in a non-dimensional frame of reference. The constants obtained upon the integration and solving of the governing relations were used to differentiate strong shocks from weak ones and likewise for the radiation strengths too.

2.3.2. One Dimensional Detonation. One dimensional steady detona--tions have been studied by the implementation of a second-order Godunov scheme of CJ waves. Sharpe et al. observed the post-shock pressures for different activation temperatures and they compared their results with linear stability analysis. The increase in activation energy was found to produce more oscillations in pressure which in turn were heavily dependent on the non-linearity of the pressure profile downstream [28]. Similar studies have also been carried out with regard to unsteady detonations where the grid resolution was found to have an effect on the oscillations of pressure downstream and on the convergence of the solution. Higher resolution was found to be beneficial [29]. High-order non-oscillatory schemes have been used to determine the effect of the computational domain size on the accuracy of results in the reaction zone. Hwang et al. determined this resolution to be at least 20 points per reaction zone half-length for accurate resolution of an overdriven shock [30].

Other works in relation to combustion behind shock waves have been more parametric in nature. Singh et al. [31] examined the ranges of pre-mixed combustion configurations, in 1-D, possible for a stoichiometric methane-air mixture to undergo a transition from diffusion-controlled to diffusionless combustion states. Their numerical study took into account a time stepping method to solve the transport, detailed chemical models and shock relations represented by finite-difference spatial

grids. Their flow solutions concentrated on the post-shock regions and proved the triviality of the role played by diffusive transport in one-dimensional steady detonation solutions even at Mach 5 shock speeds.

While the above studies have looked at detonations, they have mostly been constant-volume based models. Li et al. assumed constant pressure processes to test their JP-10 chemical kinetics models [32], [33]. Program CJ wave initially developed by Zhao, J. [34] focused on the determination of flow properties and species mass fractions downstream by neither assuming constant pressure or constant volume conditions. Griner et al. [35] discussed the effect of fuels such as acetylene, ethylene, etc. on the ignition delay characteristics using CJ wave. They found the pressure rise obtained upon the dissociation of products cannot be accurately explained without considering non-constant pressure and volume assumptions. The present study will focus on both the upstream effects and the consequent post shock solutions, determined by coupling with CJ wave [34].

2.4. IGNITION DELAY STUDIES

Ignition delay investigations have often been carried out to understand the ignition characteristics of a fuel and for the development of the involved kinetic mechanism. As pointed out by Spadacinni et al. [36], the induction period is defined by physical processes such as heating, diffusion and mixing of reactants followed by chemical processes such as pre-flame reactions. Ignition delay times have been experimentally determined using constant-volume bombs (which are heavily dependent upon the configuration of the test equipment), continuous-flow apparatus (which avoid considerations of non-uniform temperature and velocity distributions) and shock tubes. Shock tube measurements have commonly employed diluted driver gas (with helium or argon) to measure ignition delay.

Natural gas has been commonly used in gas turbines with ethane addition to methane studied more as a presence of a contaminant in the fuel. Spadacinni et al. conducted shock-tube measurements to calculate the ignition delay times for

methane-ethane mixtures and natural gas fuels [36]. The ignition delay times for methane-hydrocarbon binary mixtures were then represented by empirical relations. As is often the case with most ignition delay studies, they also performed chemical kinetics modeling to determine the ignition mechanisms. The kinetic sensitization performed by them was found to be heavily dependent on the underlying physical and chemical processes. They found methane to possess long induction times at low temperatures and thereby to require long shock tube lengths. Their studies which involved ground testing of engine performance at high Mach numbers required high inlet temperatures of air. Thus, they also studied the effect of vitiated air stream effects on ignition delay.

Similar studies were conducted by Zhang et al. [37] for $CH_4/H_2/O_2/N_2$ mixtures. They compared their results to those by other researchers for the Gas Research Institute GRI-Mech 3.0 mechanism. The ignition time for methane was found to be longer than that for other fuels due to its higher autoignition temperatures. Addition of ethane to methane showed a reduction in ignition delay times. Regression lines fit to their experimental data were based on Arrhenius-type equation based on pressure, equivalence ratio and amount of O_2 present. The equation they proposed took the following form.

$$\tau_{ign} = 3.4734 \times 10^{-4} p^{-0.788} \phi^{0.255} X_{O_2}^{-0.871} exp\left(\frac{47.312(cal/mol)}{RT}\right) \tag{6}$$

The inverse dependence of ignition time on pressure and oxygen concentration could easily be inferred from the above expression. In fact, this inverse dependence of ignition time on pressure has often been studied, with several researchers proposing different forms for this pressure variance including a near linear one [38]. Other forms of the above equation in literature show a $[C_xH_y]^n$ dependence if hydrocarbon concentrations are considered. The power dependencies of the concentration terms have been obtained more through trial and error.

The representative induction times have often taken different forms due to slight change in activation energy levels used and consequent difference in exponents for the concentration terms.

Ignition delay time is often defined by either the pressure peak or by the release of ignition precursors, intermediate free radical species in essence, such as OH^* or by CH^* chemiluminescence measurements [39]. Alternatively, it can even be defined by the interval between the arrival of the reflected shock wave and the peak OH^* emission [37]. These definitions can be tailored to suit the study at hand.

Chemical kinetics studies often supplement ignition delay measurements/ calculations as mechanisms at higher temperatures have been shown to be important in flame speed predictions and emissions predictions [39]. A common practice is to determine the reaction rate coefficient of an elementary reaction in a mechanism which is given by the equation,

$$k = AT^{\beta} exp(E/RT) \tag{7}$$

Sensitivity analysis or reaction path analysis is then carried out on the equations of interest to determine their importance in the ignition of the fuel. Sensitivity is often defined in the following form,

$$S = \frac{\partial \tau}{\partial k_i} \tag{8}$$

where a positive sensitivity indicates a faster ignition with increasing k_i. These analyses are heavily dependent upon the mechanism and the rate constants used. Modified models are then proposed by considering such reactions to be more dominating. Such has been the line of approach in ignition delay studies as can been seen from various studies in the past [37], [39]-[41]. Reactions of primary importance, inhibitive in nature, are those that consume reactive radicals such as H^* while those of secondary importance are those that produce active radicals by the combination of inactive radicals such as methyl (CH_3) and hydroperoxy (HO_2). The inhibitive reactions are necessarily endothermic [36] . Zhang et al. found that the

reactions in GRI-Mech 3.0 that consumed H^* radicals were key to the determination of ignition delay times where hydrogen addition substantially decreased the delay at high temperatures (about 1400 K) [37]. Similar acceleration in ignition process was pointed out by Petersen et al. [39] upon the addition of ethane and hydrogen to methane-based fuels.

Vasu et al. [38] determined the ignition characteristics of jet fuels such as JP-8, Jet-A and surrogate jet fuel mixtures at different equivalence ratios, oxygen concentrations, pressures and temperatures. The high fuel concentrations used resulted in detonations and thereby shortened the distance between the reflected shock wave and the combustion front. Due to the presence of detonations, their ignition times, defined by steepest rise in OH^* emission curve, were of the order of micro-seconds while previous studies, devoid of detonations, had an order of magnitude of milli-seconds for the induction time. The present study which involves detonations will attempt to study the radiation effects on ignition delay times which possess a similar order of magnitude.

3. DESCRIPTION OF PROBLEM

The previous section covered four areas of extensive research. The challenge of the present study is to coalesce all these into one executable problem. A one dimensional gray gas analysis is presented which incorporates formation of normal shock waves and combustion phenomena. The fuel-oxidizer mixture is input at conditions that would compel a shock wave to be formed. The methodology to incorporate any radiation model would then be to initially consider the emissivity characteristics of the products of combustion. The impact of this radiation in front of the shock would then depend upon the absorptivity of the reactants. Thus, the entire problem can be categorized into two computational domains viz. the downstream and the upstream regions.

3.1. THE DOWNSTREAM REGION

The fuel-oxidizer mixture conditions at the inlet of the combustor are adjusted such that a shock wave can pass through the reacting mixture. Strong detonations are produced for a sufficiently large pressure difference across the shock wave. In fact, detonations have often been looked at as shock waves followed by deflagration or as deflagration-supported shocks [42]. The flow that exists at speeds greater than the sonic velocity upstream gets transformed into subsonic flow downstream due to the presence of a shock wave. The consequent process of combustion which in essence is a heat-addition process results in acceleration of this subsonic flow (see Figure 3.1.). This acceleration however is physically not feasible when the Mach number corresponds to unity, a state of thermal choking, as the entropy of the system would have reached its maximum value. Thus, the flow downstream continues to get accelerated until thermal choking occurs.

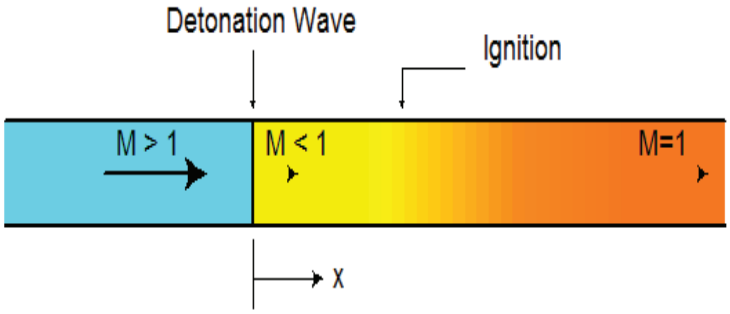

Figure 3.1. One-dimensional detonation wave model (Isaac and Scott, 2001) [33] as a shock wave followed by subsonic heat addition and choking.

The rise in temperature due to the shock wave results in the reaction to take place in the mixture which ensures the combustion wave to propagate as fast as the shock itself. The shock wave relations which help relate the inlet conditions with those prior to combustion can be expressed in a compact manner by substituting the velocity ratios for density ratios from the continuity equation, resulting in the following.

$$\frac{p_2}{p_1} = 1 + \frac{\rho_1 u_1^2}{p_1}\left(1 - \frac{\rho_1}{\rho_2}\right) \tag{9}$$

$$\frac{h_2}{h_1} = 1 + \frac{u_1^2}{2h_1}\left[1 - \left(\frac{\rho_1}{\rho_2}\right)^2\right] \tag{10}$$

The above equations can be solved in an iterative process for non-ideal gases by guessing an initial value for the density ratio and correcting it during subsequent iterations [43].

Modeling the flow in the downstream region after the shock wave necessitates the consideration of the conservation equations for multicomponent, reacting, ideal-gas mixtures. These basic equations have the following general form for conservation of mass, momentum, energy and chemical species respectively [42].

$$\frac{\partial \rho}{\partial t} + \nabla.(\rho v) = 0 \tag{11}$$

$$\frac{\partial v}{\partial t} + v.\nabla v = -\frac{\nabla.p}{\rho} + \sum_{i=1}^{N} Y_i f_i \tag{12}$$

$$\rho\frac{\partial u}{\partial t} + \rho v.\nabla u = -\nabla.q - P(\nabla v) + \rho\sum_{i=1}^{N} Y_i f_i.V_i \tag{13}$$

$$\frac{\partial Y_i}{\partial t} + v.\nabla Y_i = \frac{\omega_i}{\rho} - \frac{\nabla.(\rho Y_i V_i)}{\rho} \qquad i = 1, 2, ...N \tag{14}$$

where q in the general form is given by

$$q = -\lambda\nabla T + \rho\sum_{i=1}^{N} h_i Y_i V_i + R^0 T\sum_{i=1}^{N}\sum_{j=1}^{N}\frac{X_j D_{T,i}}{W_i D_{ij}}(V_i - V_j) + q_R \tag{15}$$

The first term in the above equation signifies conduction, the next two convection and the last term, radiative heat flux, the quantity of prime interest here. However, the incorporation of the radiative heat flux term in the energy conservation equation here results in negligible contribution between successive computational cells in the downstream region.

In order to study the non-linear variation of flow variables upstream due to q_R, the following assumptions are made. The flow is assumed to be steady and one-dimensional with negligible heat conduction and heat convection. External forces on the species are also ignored, thus reducing the problem to one that defines the radiant heat flux vector. The resultant equations that primarily possess the gradient terms can be simplified to obtain expressions for gradients of density, temperature and species' mass fractions as represented by equations 16 - 19. These equations can be solved numerically by specifying a certain step size and obtaining the quantity (density, temperature or species' mass fractions) at the node of interest. The sudden release of energy renders the equations to form a stiff matrix and

necessitate the choice of a small step of integration. In other words, the different scales of characteristic reaction times that exist in the process of combustion cause stiffness of the matrix of equations 16 - 19. The solution to such stiff matrices is obtained by using LSODE [44], [45]. The stiffness of the matrix of interest can often be detected by verifying the stiffness of the Jacobian matrix. LSODE provides the choice for the internal calculation of the Jacobian matrix or for the Jacobian matrix to be provided externally by the user. The non-zero elements of a non-full Jacobian matrix are computed internally by using difference quotients and are stored in the form of banded matrices for computational efficiency. This method of computation undoubtedly provides for a programming simplification.

The species and flow properties downstream can thus be obtained by the spatial integration of equations 16 - 19 using LSODE. This integration results in observing the equilibrium composition downstream if the numerical scheme results in successful convergence. Convergence here refers to the provision of the optimum inlet conditions for the system or rather the optimum initial values for the initial value problem.

$$\frac{d\rho}{dx} = \frac{\rho\left(T\frac{dR_{gas}}{dx} + R_{gas}\frac{dT}{dx}\right)}{\left(\frac{\rho u}{\rho}\right)^2 - R_{gas}T} \tag{16}$$

$$\frac{dT}{dx} = \frac{TT^{''}\frac{dR_{gas}}{dx} - T^{'}}{C_{p,F} - R_{gas}T^{''}} \tag{17}$$

$$where, \qquad T^{''} = \frac{u^2}{\frac{(\rho u)^2}{\rho} - R_{gas}T} \tag{18}$$

$$\frac{dY_i}{dx} = \frac{\omega_i}{\rho u} \tag{19}$$

3.2. THE UPSTREAM REGION

The radiative heat flux from the products of combustion is now to be considered for the upstream region. This upstream region poses certain challenges. One of the objectives of study, the determination of the temperature variation in front of the shock, requires the knowledge of either the temperature gradient or the boundary conditions. The slope of the temperature curve not being known *a priori* results in the determination of Dirichlet-type boundary conditions for temperature an absolute necessity and an initial starting point to obtain the desired profile.

For this analysis, the upstream region can be considered as a region of constant-area frictionless flow. The higher temperature gases downstream of the detonation wave radiate heat upstream causing temperature rise. This temperature rise due to heat addition from the products of combustion is used to determine the mixture temperature immediately upstream of the shock. The local stagnation temperature at the inlet is obtained from the local temperature and local Mach number from the equation shown below.

$$\frac{T_0}{T} = 1 + \frac{\gamma - 1}{2} M^2 \tag{20}$$

This local stagnation temperature at the inlet is related to that right in front of the shock by,

$$T_{02} = T_{01} + \Delta T_0 \tag{21}$$

This in turn could be used to determine the local Mach number, temperature, pressure and velocity by the following equations in order [46].

$$\frac{T_{02}}{T_{01}} = \left[\frac{1+\gamma M_1^2}{1+\gamma M_2^2}\left(\frac{M_2}{M_1}\right)\right]^2 \left(\frac{1+\frac{\gamma-1}{2}M_2^2}{1+\frac{\gamma-1}{2}M_1^2}\right) \tag{22}$$

$$\frac{T_2}{T_1} = \left[\frac{1+\gamma M_1^2}{1+\gamma M_2^2}\left(\frac{M_2}{M_1}\right)\right]^2 \tag{23}$$

$$\frac{T_2}{T_1} = \left(\frac{p_2}{p_1}\frac{M_2}{M_1}\right)^2 \tag{24}$$

$$\frac{T_2}{T_1} = \frac{p_2}{p_1}\frac{u_2}{u_1} \tag{25}$$

The continuity equation can be invoked to obtain the local densities and thus all flow properties will have been determined.

The term ΔT_0 in equation 21 refers to the rise in stagnation temperature due to heat addition in the system. This heat addition term in the present study relates to the radiative heat flux per unit mass of the system which can be represented as,

$$\Delta T_0 = \frac{q_R}{\rho u C_p} \tag{26}$$

The above equation shows the importance of the mass flow rate of the fluid on the rise in upstream temperature. Thus, the inlet conditions will dictate whether the upstream temperature rises appreciably. These conditions again could vary with the fuel-type. Figures 3.2 - 3.3 show the nature of this dependence of temperature rise on adiabatic flame temperature, absorption coefficient of the reactants (indicated by the various layers in the plot), inlet pressure and Mach number. The inlet temperature is assumed to be 300 K.

Clearly, the figures show that predominant rises in temperatures are observed when the flow rates and pressures are low, and flame temperatures and absorption coefficients are high. Thus the above figure establishes the limiting conditions to observe an appreciable rise in temperature due to radiative preheating. The

combination of these analytical features via numerical analyses along with the selection of suitable radiation parameters shall be investigated in the sections to follow.

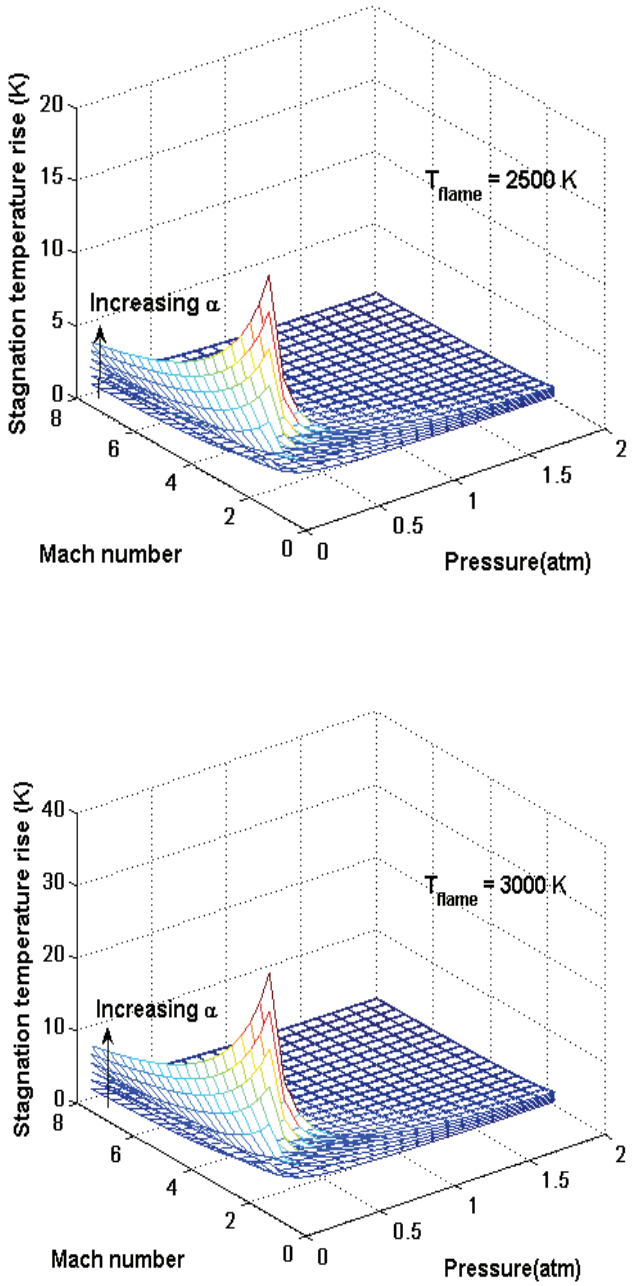

Figure 3.2. Variation of stagnation temperature rise upstream of the shock with different flow conditions and at flame temperatures of 2500 K (top) and 3000 K (bottom)

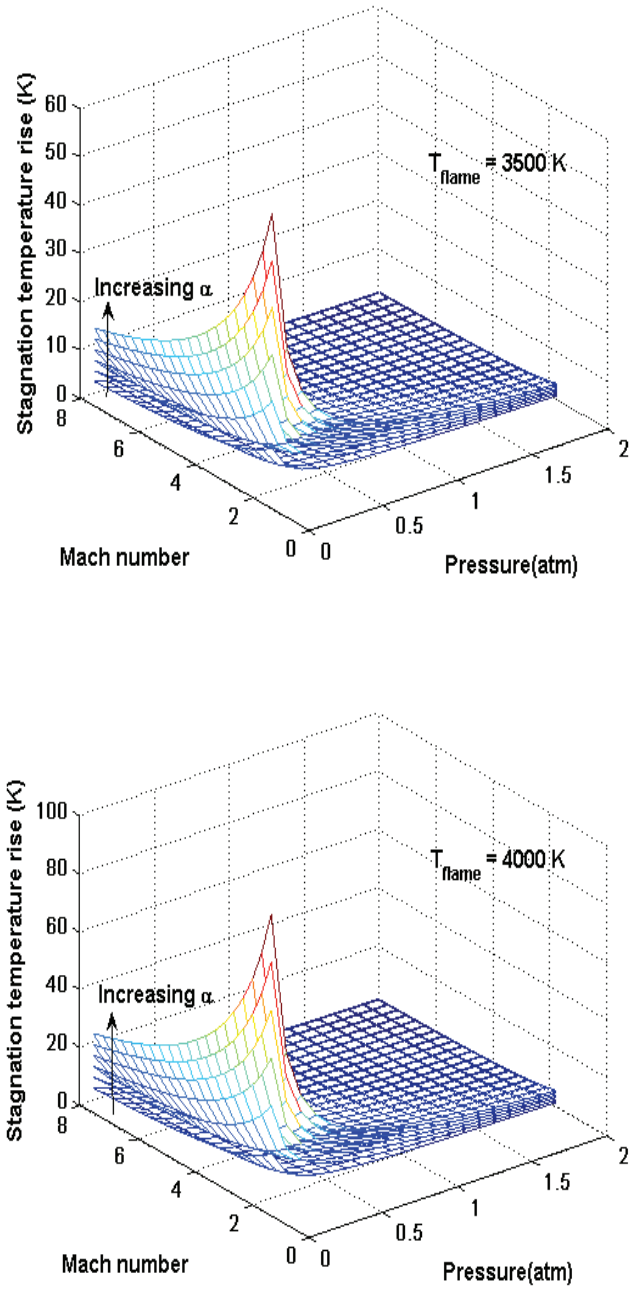

Figure 3.3. Variation of stagnation temperature rise upstream of the shock with different flow conditions and at flame temperatures of 3500 K (top) and 4000 K (bottom)

4. NUMERICAL PROCEDURE

The numerical techniques involved in observing radiative pre-heating necessitate an initial look at the techniques that have been developed previously to resolve the downstream flow.

4.1. NUMERICAL TECHNIQUES FOR DOWNSTREAM FLOW

The numerical study involves the initialization of two files, the CHEMKIN package [47] and CJwave [34] with the simultaneous coupling of various subroutines. The CHEMKIN package consists of two parts, the Interpreter and the Gas-phase subroutine. The Interpreter is initially launched in order to produce a link file corresponding to a user-defined reaction mechanism. This is subsequently linked to the gas-phase subroutine that helps in the determination of the combustion species. CJwave [33]-[35] on the other hand is the main FORTRAN code that assists in the determination of the downstream characteristics of high-speed flows including the combustion process (see Figure 4.1.).

The CJwave [34] program initializes the gas phase subroutine. It then considers user-defined input conditions such as inlet temperature, pressure and Mach number to compute the corresponding flow states behind the shock through the shock wave relations described in equations 9 - 10. The temperature and pressure conditions in particular become deterministic of combustion initiation and propagation. The flow variables are determined by solving equations 16 - 19. These gradient equations naturally depend upon the spatial discretization, dx, defined by the user. The equations which take into account the combustion process, characterized by a sudden release in energy, result in a stiff system of equations. The attainment of numerically stable solutions of this system is obtained by coupling with LSODE (Livermore Solver for Ordinary Differential Equations)[44],[45]. Thus, calling LSODE and CHEMKIN Gas phase subroutine repeatedly via CJwave [34] through a user-defined number of integration steps helps in the determination of the

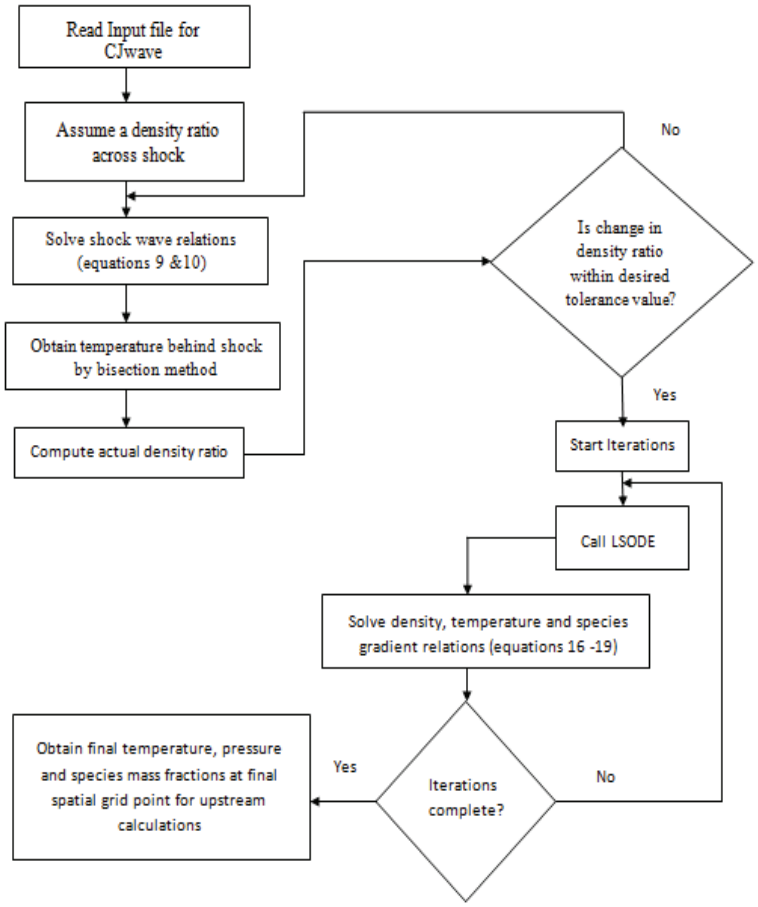

Figure 4.1. Outline of the algorithm used for downstream integration process

equilibrium composition of the products of combustion and the fluid properties in that state.

The contribution of the present study is in the development of a FORTRAN package, 'upstream_varn' (see Appendix.B), and its coupling with the above stated set of codes (Figure 4.2.) so as to obtain the radiative effects in the upstream region.

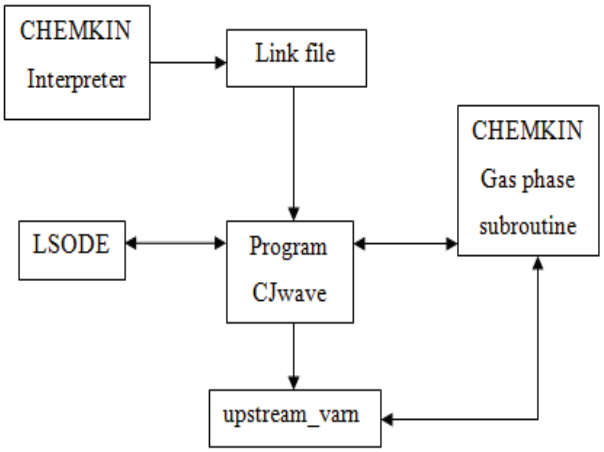

Figure 4.2. Schematic of logic flow in code package execution

4.2. METHODOLOGY-UPSTREAM REGION

The procedure to obtain the upstream variation of flow variables, temperature and heat flux in particular, begins with the quantification of the radiative heat flux incident in front of the shock due to the products of combustion behind it. This radiative heat flux helps in the determination of the rise in stagnation temperature in the upstream region as denoted by equation 21. Such a procedure entails the consideration of the downstream and upstream regions as two independent regions with fluids at comparatively different states but approximately constant properties in their own domains. The radiative heat flux is believed to be largely contributed by the major products of combustion and thus the region marching up to the ignition point and the steps following up to the attainment of equilibrium are not considered to be contributive to the heat flux due to the temperatures they possess. They, however, do play a role in the determination of the flux as they are considered in the path length calculations.

The upstream region with the boundary conditions of temperature known, is resolved into fine elements. A backward marching scheme is employed from station '2' to station '1' to determine the nonlinear variation in temperature. The heat flux at station '2' is absorbed into the first element adjacent to it (Figure 4.3.). The amount of flux depends upon the composition of the fuel mixture and the model of

absorptivity used to quantify it. The models that are considered are explained in the next section. The reduction in heat flux available for the next element is computed by the simple resultant deficit due to a partial absorption in the first element. This method is continued until the absolute error in the heat flux drops to 10^{-2} W/m^2. With the available heat flux prior to absorption being of the order of 10^7 W/m^2, the absolute error chosen results in absorption of almost the entire heat flux with an extremely low residual. This manner of flux reduction becomes definitive of the absorption length which is unknown prior to computations and as shall be seen later, a quantity of interest.

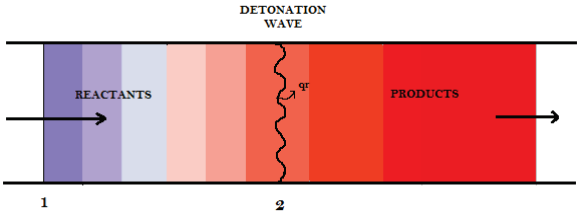

Figure 4.3. Pictorial representation of the finite volume approach used to obtain axial variation of flow properties

The temperature available for each finite volume is obtained from the basic first law of thermodynamics which relates the change in enthalpy to the change in heat addition. Thus, in terms of finite differences accurate to the first-order, this would translate to

$$\dot{m} C_{p_{i-1}} (T_i - T_{i-1}) = q_{R_i} \alpha A \tag{27}$$

For a one-dimensional analysis, the above equation would further reduce to

$$C_{p_{i-1}} (T_i - T_{i-1}) = \frac{q_{R_i} \alpha}{\rho u} \tag{28}$$

The local Mach number at every station can be obtained by a finite difference modification of equation 23.

$$\frac{T_{i-1}}{T_i} = \left[\frac{1 + \gamma_i M_i^2}{1 + \gamma_{i-1} M_{i-1}^2} \left(\frac{M_{i-1}}{M_i} \right) \right]^2 \tag{29}$$

Similarly, velocity, density and pressure at 'i-1' can be obtained by the definition of Mach number, continuity and ideal gas equations. Although the equations are inherently straight-forward, their implementation for calorically imperfect gases through coupling with CHEMKIN and CJwave pose a fair amount of complexity.

While the determination of the temperature profile through such a numerical method is initially executed, it should be noted that the temperature immediately in front of the shock is determined by assuming the entire upstream region to possess a constant temperature corresponding to that at the inlet. In other words, the determination of a nonlinear profile depends upon the boundary conditions obtained by assuming constant properties. Evidently, errors are introduced in such a determination and often reflect in the form of an asymptotic excess in the flow variable. This problem is counteracted by employing a predictor-corrector methodology. Employing such a method, which, put simply, involves a shift in the curve along the temperature-axis, requires a definition of an acceptable asymptotic error. Theoretically, as all the heat flux is not completely absorbed over a finite length of the upstream region that is used in the calculations, the temperature cannot perfectly match the inlet condition. In this study, an error of 0.1% of the flow variable was defined to be an acceptable asymptotic value. This added refinement helped in the determination of the profiles with sufficient accuracy.

4.3. EXPERIMENTAL CONSIDERATIONS TO MODEL

4.3.1. Choice of Suitable Models. The critical part of the present study involves the identification and implementation of suitable radiation parameters to quantify the radiative heat flux. Emissivity of the products of combustion requires attention at this stage. As mentioned in Section 2.2.1., several models exist to model emissivity. Near adiabatic flame temperatures generally attained for stoichiometric reactions involving hydrocarbon gaseous mixtures well exceed 2000 K. Coppalle et al. [48] determined the emissivities of high temperature flames with an accuracy of 2% over pressure-path length product ranges of 0.01 to 3.5 atm-m. As lower pressures

(generally, sub-atmospheric) and lengths of $\mathcal{O}(1\text{ m})$ are chosen in the present study, the above model was decidedly most suitable.

Coppalle's model is a modification of Hottel's [49] concept of expressing the total emissivity of a real gas in terms of a weighted sum of gray gases. The equation proposed by Hottel was of the form,

$$\epsilon_T = \sum_{i=1} a_i \left(1 - e^{-k_i p L}\right) \tag{30}$$

If ϵ_T could be represented by a function, Hottel's definition to a and k was to treat the quantities as mere numbers that could make the series representing total emissivity as given above fit the representative function. When Coppalle et al. tried to fit data for high temperature CO_2 and H_2O mixtures calculated by Edwards [50], who used exponential wide-band and statistical narrow band models, they observed a dependence of coefficients k_i and a_i on partial pressures of CO_2 and H_2O and on the flame temperature. The evolution of the weighting factors a_i, which was non-linear, was obtained by dividing the 2000 K- 3000 K temperature range into two sub-ranges, 2000 - 2500 K and 2500 - 3000 K. Their modified model for total emissivity using 1-clear and 3-gray gases fit was as follows.

$$\epsilon_T = \sum_{i=1}^{4} \left(\alpha_i + \beta_i T\right) \left[1 - e^{-k_i p L}\right] \tag{31}$$

where, the coefficients k_i, α_i and β_i were listed for different flame temperature ranges and two different ratios of partial pressure of water to that of carbon dioxide (refer Table 4.1). This formulation is particularly suitable for implementation in computer codes. It was observed that k_i was solely dependent on the partial pressure ratios while α_i and β_i showed greater variation with temperature (not seen in the partial listing). Equation 32 denotes the total radiative heat flux obtained from the products.

$$q_R = \sigma \epsilon_T T_{flame}^4 \tag{32}$$

Table 4.1. Partial listing of emissivity coefficients for a CO_2-H_2O mixture as proposed by Coppalle et al. [48]

	i	$k_i(m^{-1}atm^{-1})$	α_i	β_i
$p_w/p_c = 1$, 2000 K<T<2500 K	2	0.464	0.136	0.0000726
	3	3.47	0.516	-0.000163
	4	121.6	0.0517	-0.0000176
$p_w/p_c = 2$, 2000 K<T<2500 K	2	0.527	0.132	0.0000725
	3	3.78	0.547	-0.000171
	4	99.54	0.0489	-0.0000176

The values for partial pressure, p, and path length, L, which is usually the characteristic geometric length, as shown in equation 30, are obtained from the end state, final spatial point output of CJwave.

Absorption of radiation by ethane-air mixture can be modeled by either absorbance based $\left(A = \log_{10}\left(\frac{I_0}{I}\right)\right)$ or transmittance based $\left(T = \log_{10}\left(\frac{I}{I_0}\right)\right)$ methods. While most models in literature utilize the gas absorption of a 3.39 μm laser-beam, preference for the choice of model for this study was given to models that included a temperature dependence apart from the usual partial pressure and path length dependencies.

Olson et al. [51] defined absorptivity in terms of the amount of intensity absorbed by various hydrocarbon-argon mixtures by the relation,

$$a = \frac{\log_{10}(I_0/I)}{bc} \tag{33}$$

The absorption coefficient from the above relation was calculated in the present study by computing the product of the absorptivity, concentration and the optical pathlength. While various hydrocarbon gases were tested and temperature based correlations developed for each of them, the expression corresponding to that of

ethane was used here. The absorptivity of ethane (in cm^2 mol^{-1} units) was given by

$$a(C_2H_6) = (4.78 \pm 0.03) \times 10^4 - 10.01T - 0.0017T^2 \tag{34}$$

The models thus chosen were incorporated into the finite difference scheme wherein the local partial pressures, concentrations and temperatures were utilized for enhanced accuracy.

4.3.2. Spatial Resolution. Particular attention has to be given for the spatial resolution in the upstream region which greatly affects accuracy. The methodology proposed so far considers an upwind piecewise-constant finite difference approximation for the various flow equations (see Figure 4.4.).

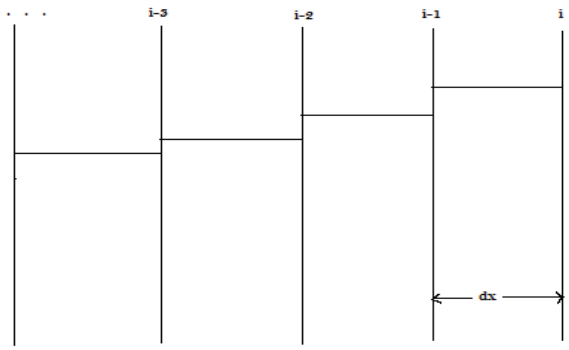

Figure 4.4. Representation of the finite volume approximation used in the present study

This formulation considers the path length for absorptivity to be defined by the step size, Δx. The value for this step size would depend upon the experimental model chosen. Typically, this would translate to the slit width of the experimental photovoltaic detector used to observe the attenuation of the laser beam. The absorption coefficient value for a computational cell width of 1 cm was obtained from Oslon's experimental path length of 9.6 cm by linear scaling. As the absorption coefficient for the path length of 9.6 cm was essentially constant, this linear scaling provided for no significant loss in accuracy. Besides, the reduction in cell width is imperative when the absorbing capacity of the upstream gas is enhanced by changing

the composition of the mixture. The importance of this point will be brought out in greater detail in later sections related to case studies.

Thus, Olson's absorptivity values obtained for a length of 9.6 cm are reduced to 1 cm to match standard absorption coefficient units. In the absence of any spectral considerations that require extremely fine resolutions [$\mathcal{O}(10^{-6}m)$], it is believed that this step size produces fairly accurate results and also provides a common platform for comparing the absorptivities of various gases.

4.4. DESIRED RESULTS

The non-existence of models that exactly match the conditions of the present study makes validation a difficult task. Nevertheless, a couple of models in literature can be referred to for an understanding of the qualitative expectation from the present study. One such work is that by Heaslet and Baldwin [6] as described in Section 1.1. Their numerical results were restricted to very specific shock and radiation strengths (Figure 1.2.). The radiation strengths obtained from combustion processes are lesser in comparison to those utilized by them. The upstream temperature variation that they obtained for strong shocks and weak radiation gives an initial insight into what could be expected for the present study.

Astrophysical studies on radiative shocks have also focused on this upstream temperature variation. Drake [52] studied the effect of optically thick (large optical depth) radiative shocks on upstream and downstream temperature. The radiative shocks used in their study which signify large spatial scales resulted in an upstream variation that was categorized into two separate, broad regions. The first region where local emission was insignificant displayed an exponential increase in temperature. This region was called the "transmissive precursor". The next region to follow was the "diffusive precursor" which was formed due to heating from a constant temperature source. The temperature downstream was considered to decay off into a "cooling layer".

The presence of combustion processes in the present study precludes the existence of the cooling layer downstream. High mass flow rates and high Mach numbers of this study prevent the diffusive precursor region from existing. Hence, the transmissive precursor indicates a temperature variation that is most relevant to the present study (see Figure 4.5.). The focus therefore would be to observe this monotonically increasing trend of temperature upstream of the shock.

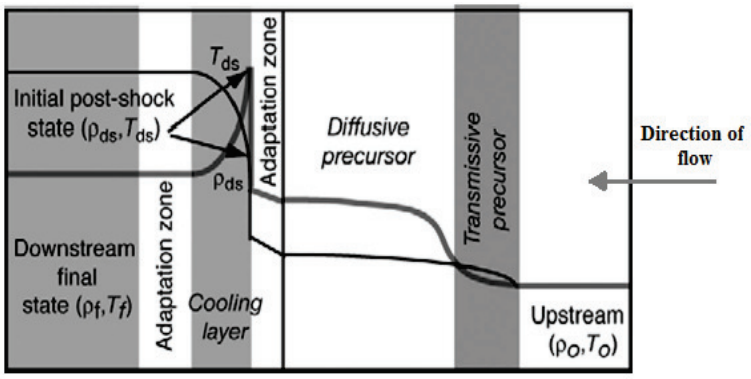

Figure 4.5. Schematic of optically thick radiative shock as put forth by Drake [52]

With the understanding of the above background on radiative transfer through gray gases and the implementation of those concepts through numerical analyses, the outcome of using such numerical methodologies shall be examined to analyze flow behavior upstream and downstream of a detonation wave.

5. RESULTS AND DISCUSSION

Program CJwave [34] previously was executed for different stoichiometric ratios of methane-air fuel mixtures and hydrogen-air mixtures [33]. Similarly, other attempts to understand the invalidity of constant-pressure and constant-volume assumptions during detonations considered acetylene-air, ethylene-air and JP-10 fuel mixtures [35]. The present study with its focus on developing a radiative heating model was conducted by considering ethane as the hydrocarbon gas in the fuel-air mixture.

Inlet conditions such as an inlet pressure of 0.1 atm, temperature of 300 K and Mach number of 7.4 was chosen for the initial case of ethane-air fuel mixture. These conditions, especially that of the Mach number were chosen to suit all case studies that were done. The Mach number is particularly deterministic of the convergence of the solution and in the determination of the equilibrium composition of the product mixture. The flow downstream of the shock wave and the subsonic Mach number immediately behind the shock is used in the forward marching scheme of CJwave in order to determine the flow variables and species composition. This process which includes the combustion process, a heat-addition process, causes the acceleration of the flow. The subsonic flow thus has a natural tendency to transition to a state of thermal choking if the process provides the necessary conditions. If this choked state signifying the maximum entropy state is attained even before the combustion process is complete due to the downstream temperature and heat provided by the mechanism, the equilibrium composition and equilibrium-state flow variables cannot be attained. This is independent of the step size chosen and is dictated by the physics, not an artifact of the numerical procedure.

The following results were obtained when ethane and air constituting 21% oxygen, 79% nitrogen by volume was used as the fuel mixture. The flow variables were normalized with respect to the upstream values. The step size chosen for this case was 5.0×10^{-3} cm. It can be seen in Figure 5.1. that temperature and pressure

show a gradual variation to attain the equilibrium-state values thereby exhibiting the capability of CJwave to capture the combustion process with fine resolution. Similar nature of variation can also be observed for density, Mach number and velocity of the product-mixture but are quite indistinguishable in Figure 5.1. due to their small magnitudes. Convective time, as depicted in the graph below, refers to the time taken by a fluid particle to travel from the detonation wave front to a position 'x' downstream [33].

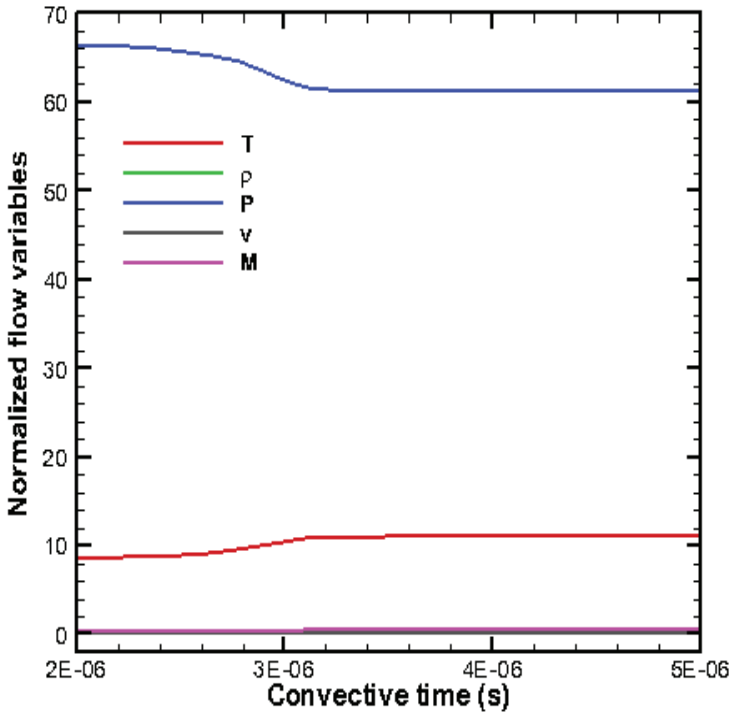

Figure 5.1. Case A: Variation of flow properties for ethane-air fuel mixture

The process can be better understood by analyzing the cross-section of species in the downstream region. A reference to the reaction mechanism used would be vital to the understanding of the behavior of species as shown in Figures 5.2 and 5.3.

DRM 19 mechanism [53] which is a subset of the GRI-MECH 1.2 mechanism [54] was used here. The mechanism involves '19' active species apart from inert species such as N_2 and Ar, and 84 reactions. It can be seen that at close to 3μs, the

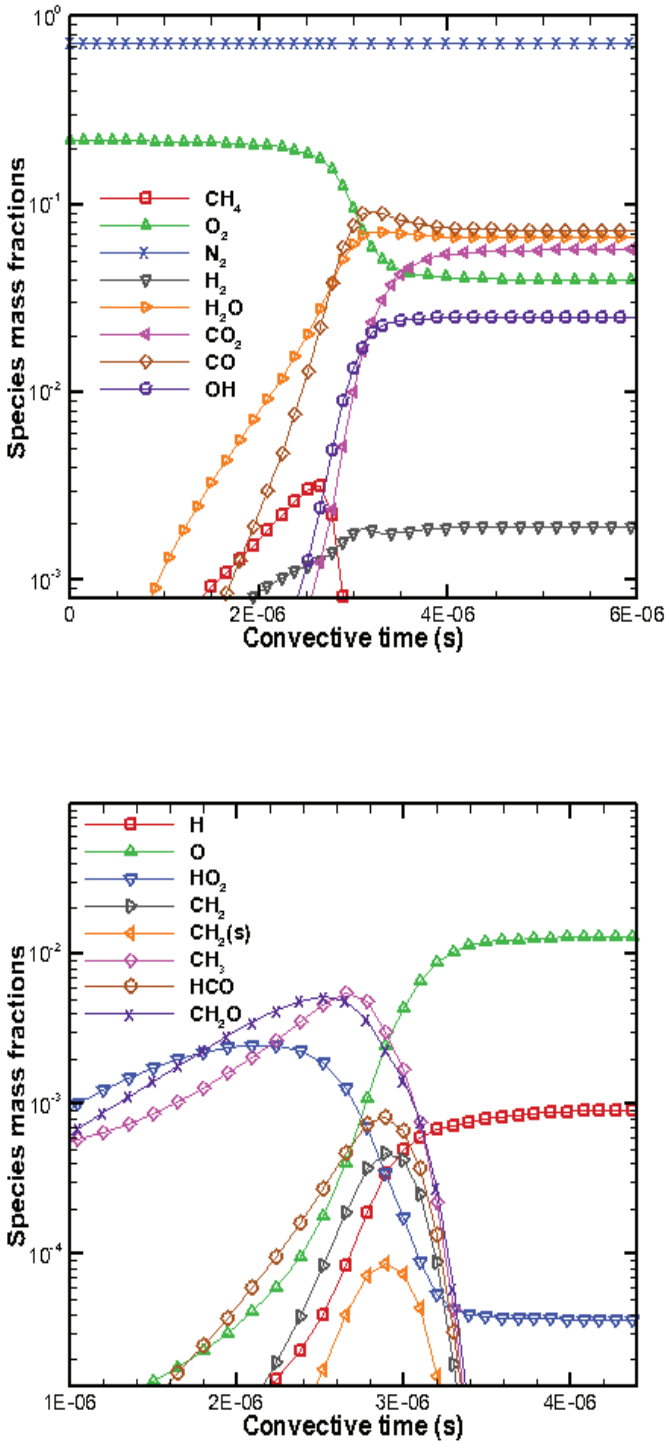

Figure 5.2. Case A: Variation of species mass fractions for ethane-air fuel mixture for the first 16 species in the DRM 19 mechanism

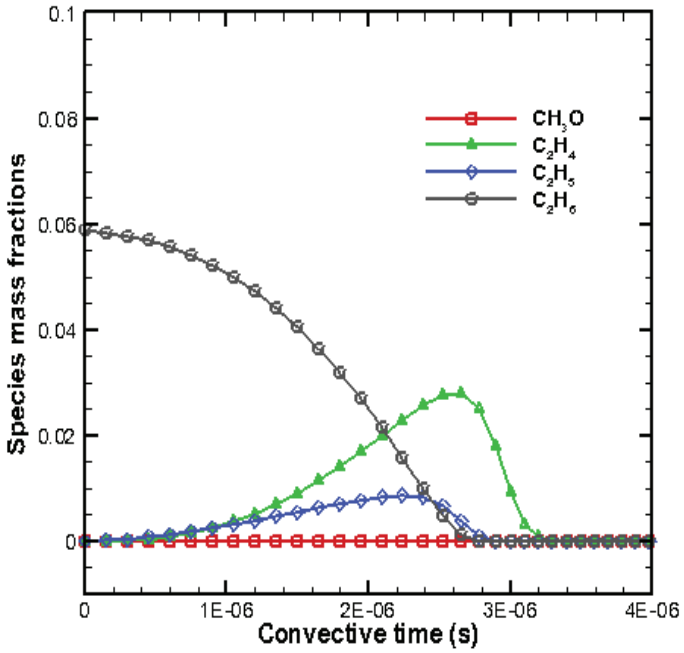

Figure 5.3. Case A: Variation of species mass fractions for ethane-air fuel mixture for the last four species in the DRM 19 mechanism

reaction approaches completion. This is characterized by C_2H_6, O_2 getting consumed almost entirely and species such as CO and H_2O reaching their peak values. It is interesting to note that CO_2 does not peak at the same instant as H_2O. This is due to the fact that the major limiting reactions (distinguishable by the activation energy values of the Arrhenius coefficients provided in the mechanism file) producing H_2O do so by consuming OH. These reactions form the initial part of the mechanism. H_2 and CO reach their peak values once CH_2O gets completely consumed. These species require the highest activation energy for the reaction to proceed. The high values of CO in the product mixture at this point results in it combining with HO_2 to produce large quantities of CO_2. The peak value of carbon dioxide is attained only after OH production has peaked. Thus, the slight offset in the major species' mass fraction values are due to the nature of reactions in DRM 19 mechanism. The flow variables reach their equilibrium state values as CO_2 reaches its peak value.

With this understanding of the downstream behavior of the flow, the upstream temperature and heat flux were quantified using the subroutines developed in 'upstream_varn' (see Figure 5.4). The equilibrium state value for the downstream temperature was 3300 K. The attainment of this high value is due to the high speed of the flow in the upstream region and the consideration of the stoichiometric nature of the reaction. Thus, hydrocarbon-gas mixtures that under standard conditions of temperature and pressure produce flame temperatures of magnitudes lesser than 3000 K can under the influence of a shock wave produce greater flame temperatures. The heat flux corresponding to this temperature value was of $\mathcal{O}(10^6 W/m^2)$. The step size chosen, after 22000 iterations, resulted in a path length of 1.1 m. The equilibrium-state value of the downstream pressure was 0.6 atm. The resultant pressure-path length product of 0.67 atm-m rendered the usage of Coppalle's model valid for the present study.

The complete absorption of heat flux available in front of the shock took place over a distance of close to 6 m as the upstream temperature dropped to the pre-defined asymptotic value of 300.3 K. This rise in upstream temperature if updated for the downstream flow resulted in a downstream temperature of 3273 K. That would amount to a 0.8% reduction in downstream temperature due to the radiative heating upstream. The above results were treated as a base case in order to understand the effects of parametric variation of the fuel composition on upstream heating.

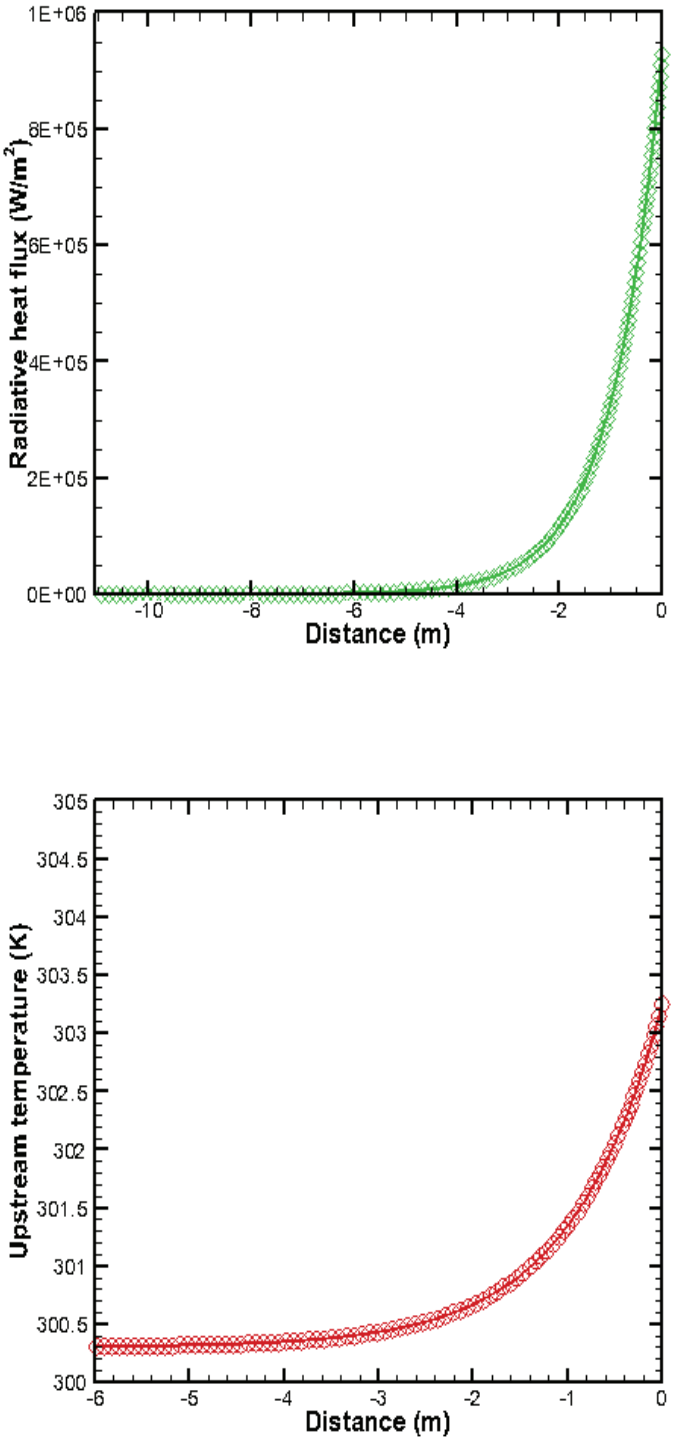

Figure 5.4. Variation of radiative heat flux and temperature upstream for ethane-air fuel mixture

5.1. CASE STUDIES

The case studies presented here can be categorized into three types. The first being the variation of the inert gas present in the reactants. The second involved the study of variation in upstream inlet pressure and the last of the case studies involved dilution of the reactant mixture with different polyatomic gases.

5.1.1. Variation of Nitrogen Concentration in Air. Case A presented earlier used the standard composition of air i.e. 21% oxygen 79% nitrogen by volume. It was of interest to observe the effect of increasing O_2 concentration in the upstream region on the temperature profile. As per the mechanism, large volumes of O_2 combine with CO to yield O and CO_2. Higher oxygen concentrations could lead to greater production of CO_2 in the product mixture. Also, a dominant reaction in the mechanism is the combination of H radical with O_2 to form OH, a specie of interest in defining the ignition delay characteristics under the prevailing conditions. Five variations of this composition of air were considered and the upstream temperature profiles were studied (see Figure 5.5).

Higher O_2 in the fuel mixture leads to development of greater partial pressures of the gas immediately in front of the shock. This component being critical in the determination of the absorption coefficient of the reactant mixture leads to the development of steeper curves for temperature. The case without any inert gas and oxygen as the only oxidizing component showed a 50% reduction in the length required to absorb the radiative heat flux in comparison with Case A. This reduction in length is a parameter of importance from point of view of practical applications. The length of the combustor would typically encompass both the upstream and downstream regions. Such a detonation-based combustor would certainly be viable if the upstream region is shorter or at least of the same length as the downstream region.

The case of ethane gas and pure O_2, due to the added competitiveness it displays with respect to Case A, deserves more attention. This case, Case B for future references, shows higher magnitudes of flow properties as seen in Figure 5.6.

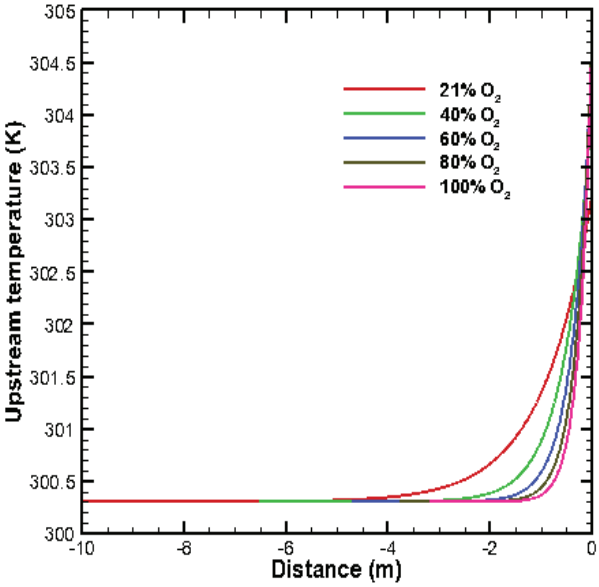

Figure 5.5. Variation of upstream temperature for different O_2/N_2 compositions of air

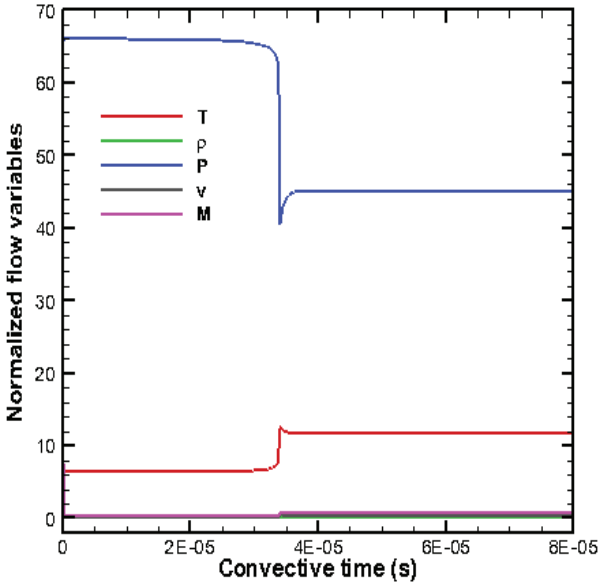

Figure 5.6. Case B: Variation of flow properties for ethane-oxygen fuel mixture

An apparent difference between Cases A and B is in the slight overshoot in normalized temperature and undershoot in normalized pressure curves. This is a consequence of the physical process. The grid size chosen is highly resolved in order to capture the explosive nature of the combustion process. The depiction of grid points would closely follow the path of the flow curves leaving the points and the line indiscernible. The critical reactions in the DRM 19 mechanism to a large extent consume O_2 as shown in Table 5.1.

Table 5.1. Critical reactions involving the consumption of O_2 in DRM 19 mechanism [53]

Reaction	A (cm^3/mol/s)	n	E_A (cal/mol)
$O_2 + CO \Leftrightarrow O + CO_2$	2.500E+12	0.000	47800.00
$O_2 + CH_2O \Leftrightarrow HO_2 + HCO$	1.000E+14	0.000	40000.00
$H + O_2 \Leftrightarrow O + OH$	8.300E+13	0.000	14413.00
$CH_2 + H_2 \Leftrightarrow H + CH_3$	5.000E+05	2.000	7230.00
$CH_2 + CH_4 \Leftrightarrow 2CH_3$	2.460E+06	2.000	8270.00
$CH_3 + O_2 \Leftrightarrow O + CH_3O$	2.675E+13	0.000	28800.00
$CH_3 + O_2 \Leftrightarrow OH + CH_2O$	3.600E+10	0.000	8940.00

The temperature dependence of the rate of a reaction is commonly expressed in the following Arrhenius form.

$$k = AT^n \exp(-E_A/RT) \tag{35}$$

The activation energy, E_A, in the Boltzmann factor above represents the minimum amount of energy required by the colliding molecules for the reaction to take place. Hence, the above reactions are limiting in the sense that they have to overcome a large energy barrier (see Figure 5.7). However, once they are overcome, the forward

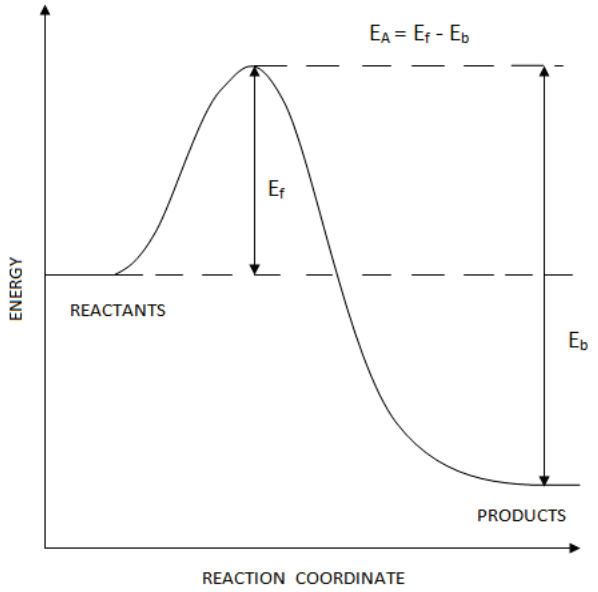

Figure 5.7. Schematic of variation of energy with the reaction coordinate for a system as represented by Glassman [55]

reactions proceed to completion, resulting in the release of energy over a short period of time. This is responsible for the sudden peak in temperature and Mach number (that is less pronounced than temperature), and the sudden dip in pressure and density (again less prominent). Once the reactions represented in Table 5.1. are complete, the consumption of the radicals formed above results in a revival of the flow properties to their equilibrium state values. This process is further substantiated by the behavior of species downstream as shown in Figures 5.8 and 5.9. Higher mass fractions of radicals can be attributed to the larger quantities of oxygen present in the reactant-mixture.

The presence of large quantities of oxygen result in a slower reaction time, almost by an order of magnitude in comparison with Case A (Figures 5.2 and 5.3.). The activation energy needed for the larger quantities of oxygen present results in this larger time to completion of combustion.

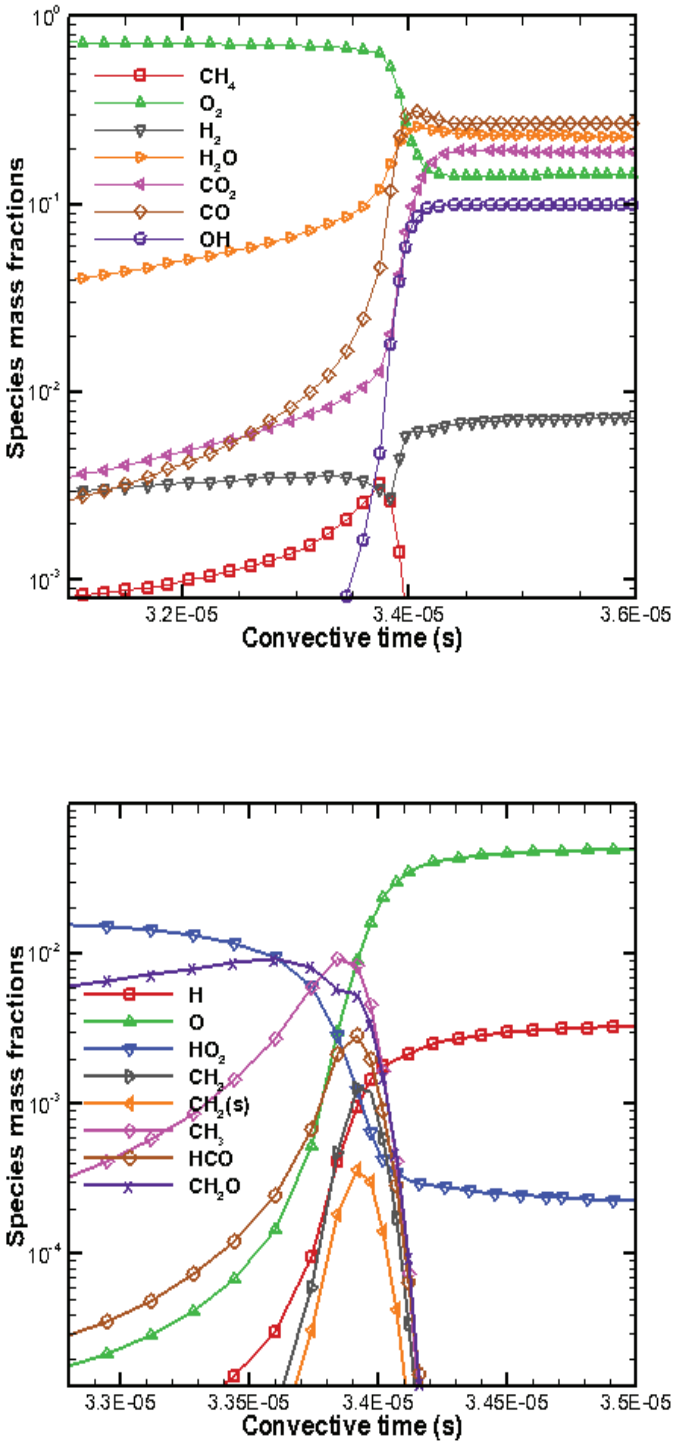

Figure 5.8. Case B: Variation of species mass fractions for ethane-oxygen fuel mixture for the first 16 species of the DRM 19 mechanism

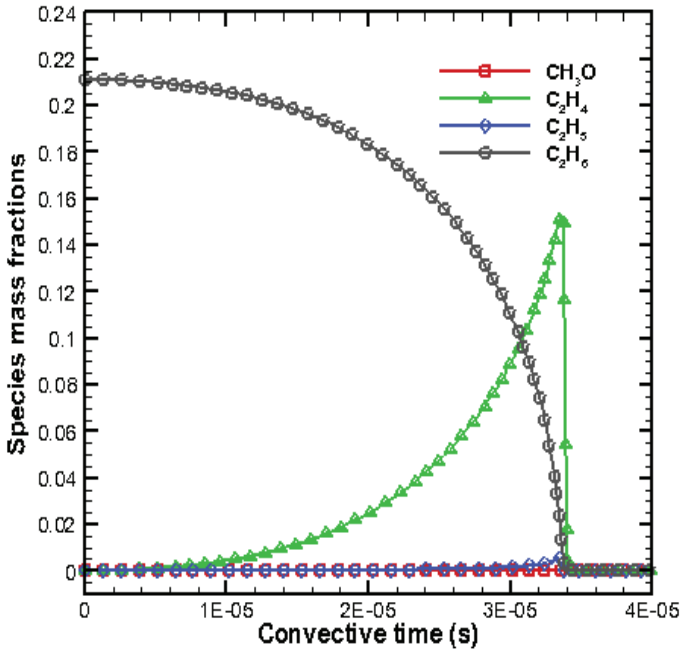

Figure 5.9. Case B: Variation of species mass fractions for ethane-oxygen fuel mixture for the last four species of the DRM 19 mechanism

5.1.2. Pressure Variation. The next set of case studies concentrated on the effect of different inlet pressures on the downstream flow and upstream absorption. Case B at 0.1 atm was chosen as the reference for subsequent variations in pressures of 0.5 atm, 1atm and 1.2 atm. Figures 5.10 and 5.11 show the variations in the upstream temperature profiles and the maximum temperature rise upstream respectively. Pressure, in the range chosen, has a more dramatic effect than varying O_2 content. A variation in upstream temperature right in front of the shock and the distance it takes to reach the asymptotic value can be observed. The absorption length depends upon the partial pressures of the reactants which increases with increasing inlet pressures. Thus, the rate of absorption is higher for 1.2 atm inlet pressure than for 0.1 atm.

Emissivity is a function of the downstream pressure and temperature after combustion is complete. The increase in inlet pressure leads to an increase in flame

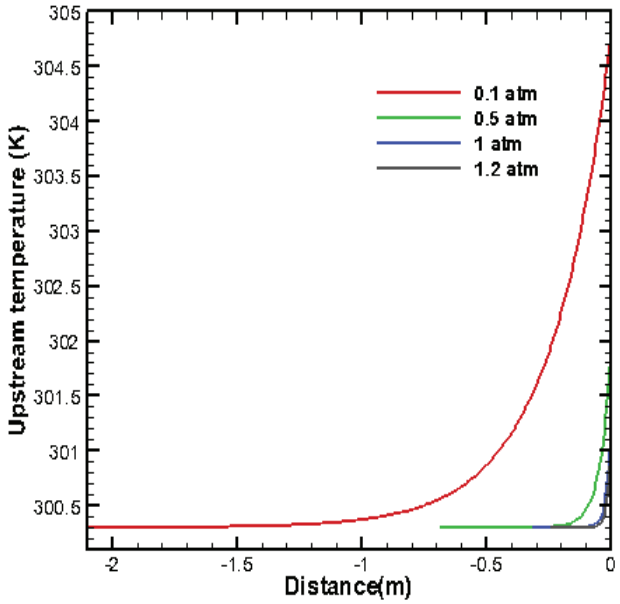

Figure 5.10. Variation of upstream temperature curves for different inlet pressures of fuel mixture

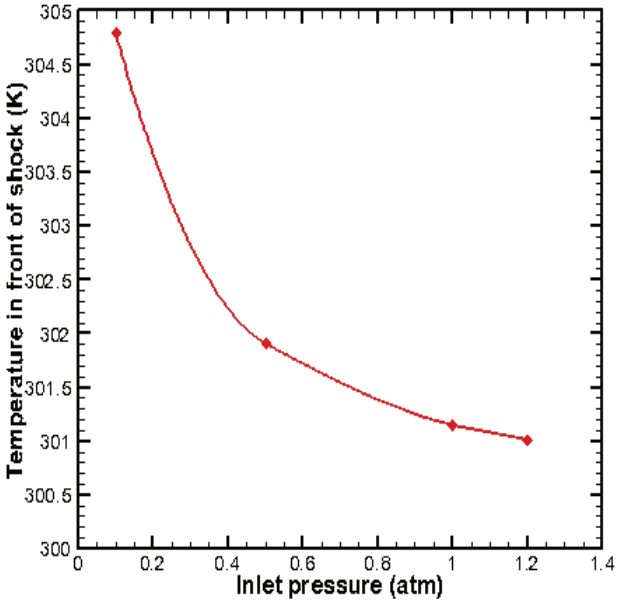

Figure 5.11. Variation of upstream temperature in front of shock for different inlet pressures of fuel mixture

temperature and downstream pressure as shown in Figure 5.12., 5.13., and the inverse exponential dependence on pressure (Eqn. 31) results in larger emissivity from the products to the upstream region. However, stagnation temperature rise upstream has an inverse dependence on pressure (Eqn. 26). Thus, increasing the pressure at the inlet has an inverse effect on the upstream temperature variation (see Figure 5.14).

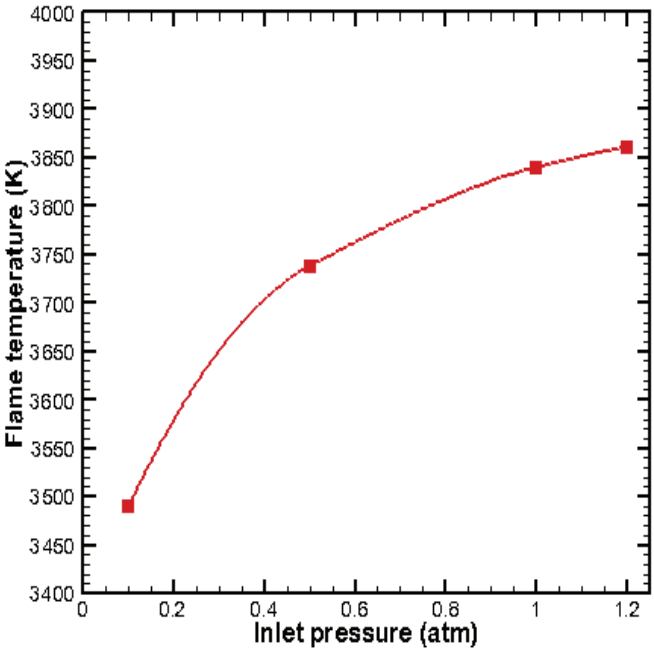

Figure 5.12. Variation of flame temperature for different inlet pressures of fuel mixture

DRM 19 mechanism contains certain pressure-dependent reactions, all of which have been listed in Table 5.2. In essence, these reactions are favored when the pressure is increased. A common characteristic that can be observed is that energy is transferred to a radical from a third body, 'M'. As can be seen, the energy required for the dissociation of ethane is substantially less than that required for reactions mentioned earlier. Thus, the reaction proceeds at a faster rate. Increasing the pressure from 0.1 atm to 1.2 atm reduces the time to attain peak values of C_2H_4 by more than an order of magnitude.

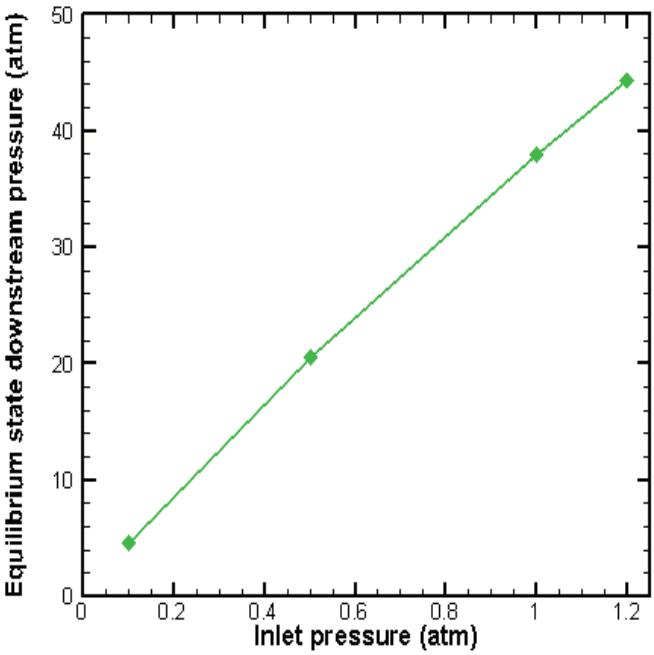

Figure 5.13. Variation of downstream pressure for different inlet pressures of fuel mixture

Table 5.2. Pressure-dependent reactions in DRM 19 mechanism [53]

Reaction	A (cm^3/mol/s)	n	E_A (cal/mol)
$H + CH_2(+M) \Leftrightarrow CH_3(+M)$	2.500E+16	-0.800	0.00
$H + CH_3(+M) \Leftrightarrow CH_4(+M)$	1.270E+16	-0.630	383.00
$H + HCO(+M) \Leftrightarrow CH_2O(+M)$	1.090E+12	0.480	-260.00
$H + CH_2O(+M) \Leftrightarrow CH_3O(+M)$	5.400E+11	0.454	2600.00
$H + C_2H_4(+M) \Leftrightarrow C_2H_5(+M)$	1.080E+12	0.454	1820.00
$H + C_2H_5(+M) \Leftrightarrow C_2H_6(+M)$	5.210E+17	-0.990	1580.00
$H_2 + CO(+M) \Leftrightarrow CH_2O(+M)$	4.300E+07	1.500	79600.00
$CH_3 + CH_3(+M) \Leftrightarrow C_2H_6(+M)$	2.120E+16	-0.970	620.00

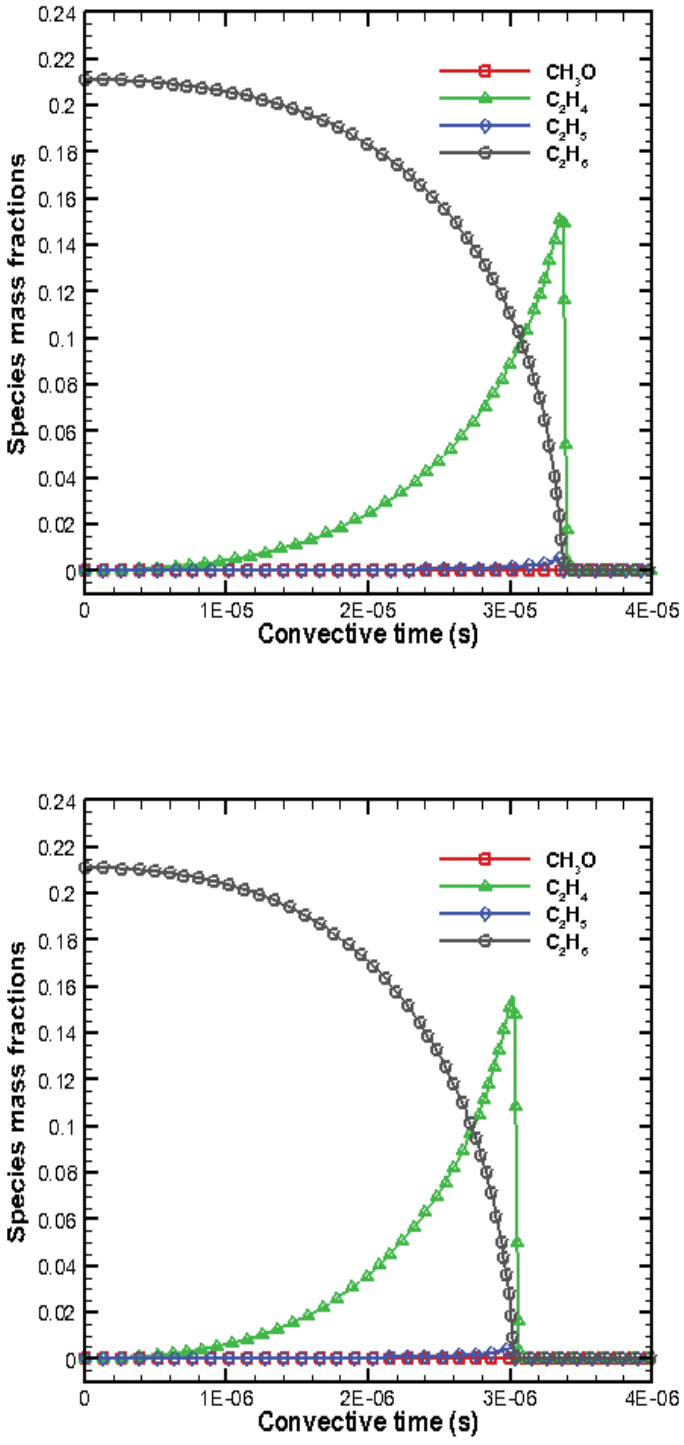

Figure 5.14. Shift in peak C_2H_4 values with varying inlet pressures of 0.1 atm (top) and 1.2 atm (bottom)

5.1.3. Dilution of Fuel Mixtures. The results from Case B throw light on the improvement of absorptivity of the fuel-mixture as the concentration of ethane was increased. The focus of the present set of case studies is to identify conditions that would improve the absorptivity of the upstream mixture by introducing polyatomic gases and minimizing the quantity of diatomic molecules such as O_2; O_2 is considered to be almost transparent to radiation. While several gases fit the criterion for testing, it was of interest to observe the effect on absorptivity if the products of combustion, particularly the major species such as CO_2 and H_2O, were to be mixed with the incoming gaseous fuel mixture.

5.1.3.1. Dilution with carbon dioxide. The absorption characteristics of carbon-dioxide to He-Ne laser radiation have been well documented by Schneider et al. [56]. They utilized the laser beam at 4.2 μm for studying the absorptivity characteristics of pure carbon dioxide as it was believed that the laser radiation at this frequency was strong in comparison with the absorption peaks of CO_2 at this wavelength. For a 2 cm path length, they obtained an absorption coefficient value for CO_2 to be 0.084 $cm^{-1}atm^{-1}$. The introduction of carbon-dioxide in the reactants was made on a percentage volume in air basis. The distribution of components in the "air" chosen was O_2 and CO_2. The volume percentages of CO_2 were varied from 10% to 40% in steps of 10. The variation in upstream temperature profiles obtained is shown in Figure 5.15.

The absorption coefficient values for CO_2, not being substantially high in comparison with ethane gas, results in profiles that do not vary a great deal from Case B. The curves shown above indicate a longer absorption distance for increasing concentrations of CO_2 in the reactant mixture. This seems counter-intuitive at first but can be understood by observing the flame temperature variations initially. The increase in CO_2 upstream results in a corresponding rise in its levels downstream too. As the CO_2 concentration levels are increased from 10 to 40% in air, the flame temperature reduces by 6.7% (see Figure 5.16). Thus, correspondingly the

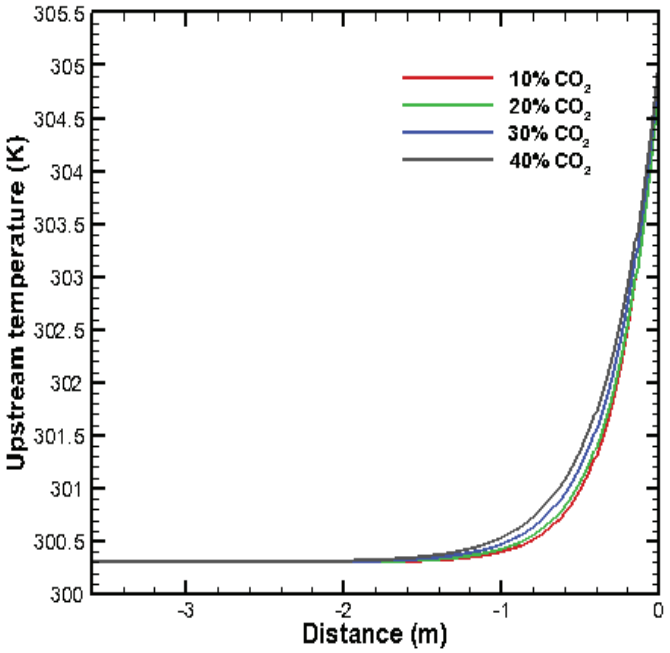

Figure 5.15. Variation in upstream temperature profiles for different dilution levels of CO_2

temperature values in front of the shock reduce by a small extent. This, however, still is only a small contribution to the variation in trends as seen in Figure 5.15. The more dominant effect responsible for this variation arises from the fact that the absorption coefficients of ethane and carbon dioxide are of comparable magnitude. The values are greatly affected by the concentration levels of the gases. Hence, as the amount of CO_2 increases, the overall absorption coefficient of the reactant mixture as indicated by the equation below, reduces. A longer absorption length ensues.

$$\alpha_{reactant-mixture} = \alpha_{C_2H_6} X_{C_2H_6} + \alpha_{CO_2} X_{CO_2} \tag{36}$$

The variation in concentrations in the downstream region is indicated in Figure 5.17. for concentration levels of 10% and 40%. Evidently, higher values of CO_2 are present when its concentration upstream in air is 40%.

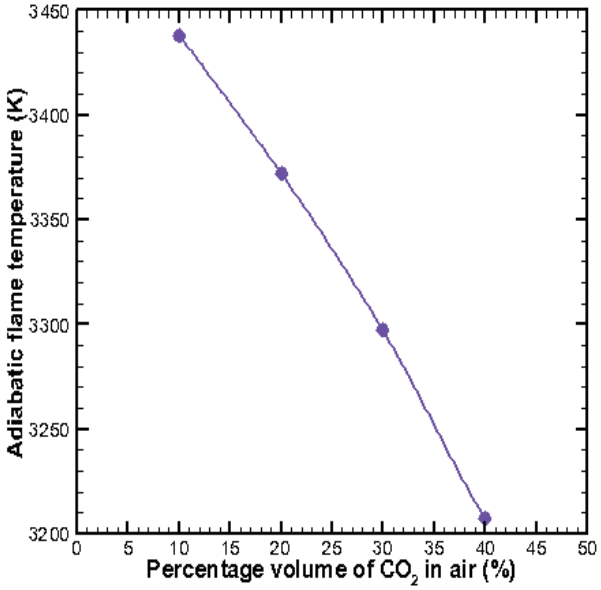

Figure 5.16. Variation in flame temperature with different dilution levels of CO_2

OH levels show a greater shift than CO levels as the consumption of CO by O_2 requires a significantly higher amount of energy while the production of OH from CO requires the necessity to overcome a smaller barrier. Table 5.3. indicates the reactions in DRM 19 that involve CO_2 production with positive activation energy values.

Table 5.3. Reactions producing CO_2 in DRM 19 mechanism and possessing positive activation energy values [53]

Reaction	A (cm^3/mol/s)	n	E_A (cal/mol)
$O + CO + M \Leftrightarrow CO_2 + M$	6.020E+14	0.000	3000.00
$O_2 + CO \Leftrightarrow O + CO_2$	2.500E+12	0.000	47800.00
$OH + CO \Leftrightarrow H + CO_2$	4.760E+07	1.228	70.00
$HO_2 + CO \Leftrightarrow OH + CO_2$	1.500E+14	0.000	23600.00

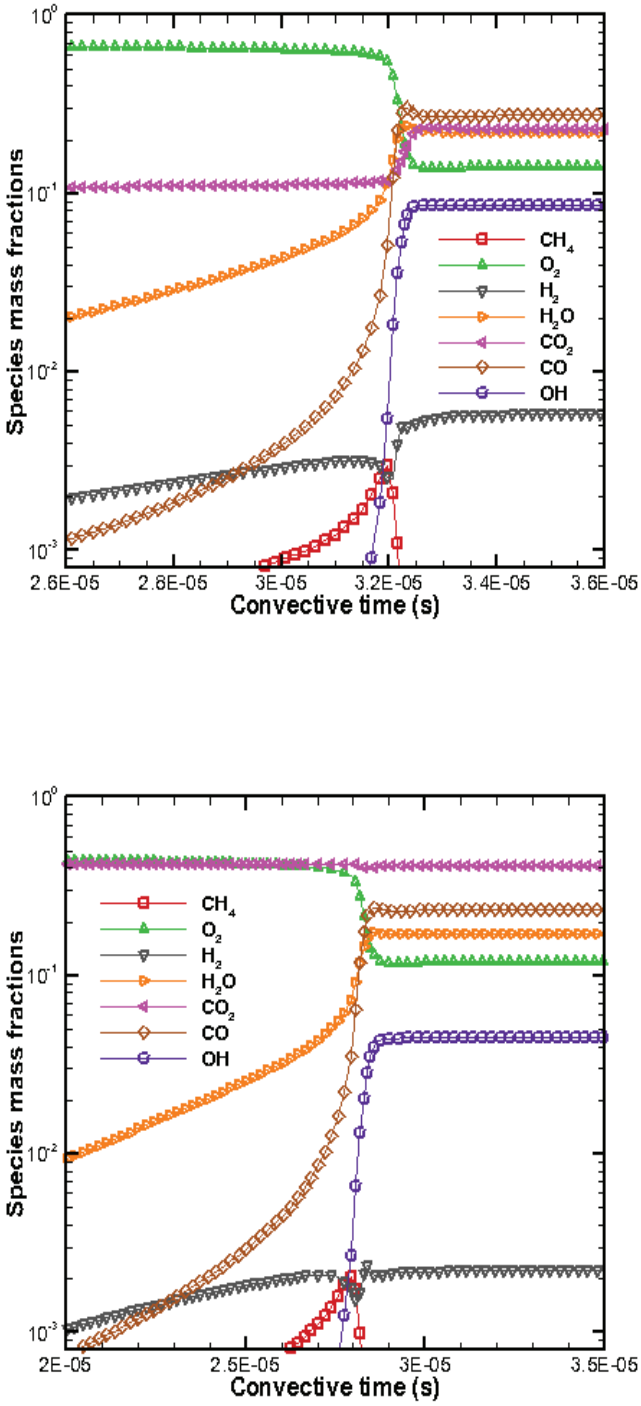

Figure 5.17. Shift in peak OH values with varying dilution levels of CO_2 in the reactant mixture of 10% (top) and 40% (bottom) in air

The presence of higher CO_2 levels also produces a shift in the time taken to reach peak CO values. A 14.9% decrease in this time was observed when the dilution levels were increased from 10% to 40%.

5.1.3.2. Dilution with water vapor. Similar efforts were undertaken to observe the effect of water vapor dilution in the reactant mixture on the upstream absorption capacity and the absorbing length. The extinction coefficient quantification of 33-μm laser radiation by water vapor as defined by Kucerovsky et al. [57] was used here. The 33-μm laser line was chosen as the desired strength as it was close to peak water vapor absorption lines. They found strong laser attenuation amounting to a reduction in radiation by $1/e$ in 6 cm of air. The extinction coefficient value they suggested was 1.548 ± 0.039 Torr^{-1} m^{-1}. The error band of this range was neglected in order to compute the absorption coefficient in each computational cell. The absorption coefficient of the mixture now was transformed to,

$$\alpha_{reactant-mixture} = \alpha_{C_2H_6} X_{C_2H_6} + \alpha_{H_2O} X_{H_2O} \tag{37}$$

The variation in upstream temperature profiles is shown in Figure 5.18. While the curves show more variation from each other, as against the case of carbon-dioxide dilution (Figure 5.15.), a couple of more important and different behaviors are observed.

The first distinct observation that can be made is a 50% decrease in the absorbing length from $\sim$2 m for carbon-dioxide case studies to $\sim$1 m for the present set. The other observation is the reversal of variance seen when carbon dioxide was used upstream. The curves become more steep with increasing water vapor dilution levels. Both these findings can be attributed to the absorption coefficient values of water vapor being higher than that for ethane. As a result, increasing concentrations of water vapor result in increasing mixture absorption coefficient. The subsequent profile behavior is a natural consequence.

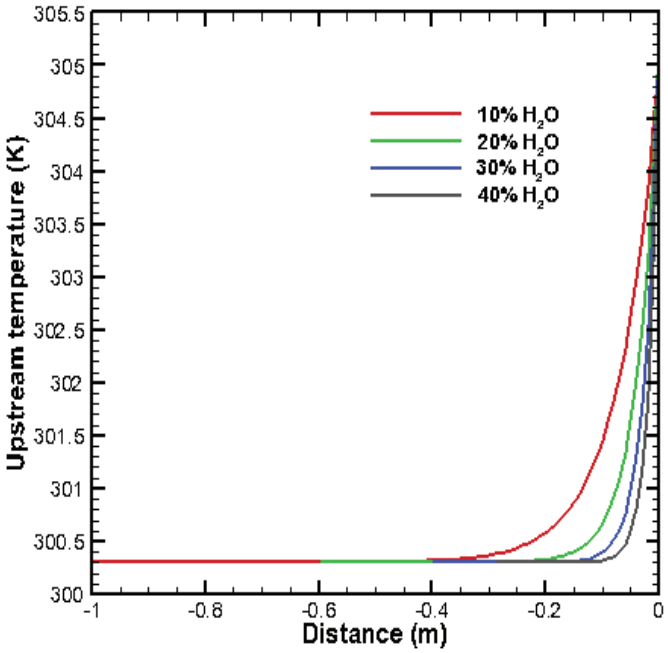

Figure 5.18. Variation in upstream temperature profiles for different dilution levels of H_2O

The downstream cross-section of species reveals predictable variations in mass fractions of H_2O and O_2. The decrease in OH mass fraction values directly correlate to higher H_2O values. A large majority of reactions in DRM 19 producing H_2O result from the combination of OH with another species. This is clearly deducible from Table 5.4. Upon the attainment of required energy, the reaction proceeds quickly to produce H_2O. The presence of H_2O in the reactants provides for easy production of OH. Thus, the time required to attain OH peak reduces by 63.5 % as the dilution levels of air by H_2O is increased from 10% to 40% (see Figure 5.19).

The addition of CO_2 and H_2O to the reactant mixture alters the downstream species concentrations as they play a role in the involved kinetics. Thus addition of any active specie to the reactant mixture results in a change in ignition delay and species mass fractions. This can be substantiated by the addition of CO, another active specie in DRM 19.

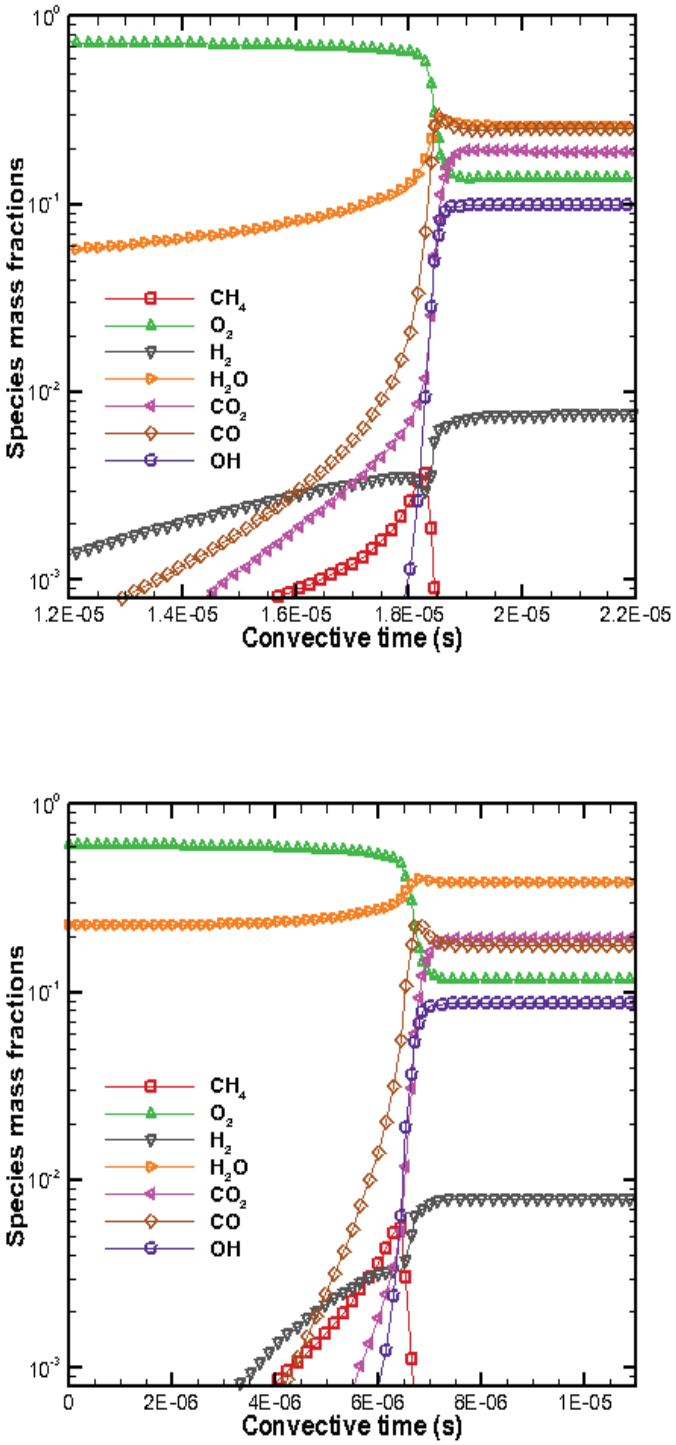

Figure 5.19. Shift in peak OH values with varying dilution levels of H_2O in the reactant mixture of 10% (top) and 40% (bottom) in air

Table 5.4. Reactions producing H_2O in DRM 19 mechanism and possessing non-zero activation energy values [53]

Reaction	A (cm^3/mol/s)	n	E_A (cal/mol)
$OH + H_2 \Leftrightarrow H + H_2O$	2.160E+08	1.510	3430.00
$2OH \Leftrightarrow O + H_2O$	3.570E+04	2.400	-2110.00
$OH + HO_2 \Leftrightarrow O_2 + H_2O$	2.900E+13	0.000	-500.00
$OH + CH_3 \Leftrightarrow CH_2 + H_2O$	5.600E+07	1.600	5420.00
$OH + CH_4 \Leftrightarrow CH_3 + H_2O$	1.000E+08	1.600	3120.00
$OH + CH_2O \Leftrightarrow HCO + H_2O$	3.430E+09	1.180	-447.00
$OH + C_2H_6 \Leftrightarrow C_2H_5 + H_2O$	3.540E+06	2.120	870.00
$HCO + H_2O \Leftrightarrow H + CO + H_2O$	2.244E+18	-1.000	17000.00

Figure 5.20 shows the effect of addition of CO on the downstream composition. The addition of CO results in faster reaction times as compared to H_2O and CO_2 (Figure 5.21).

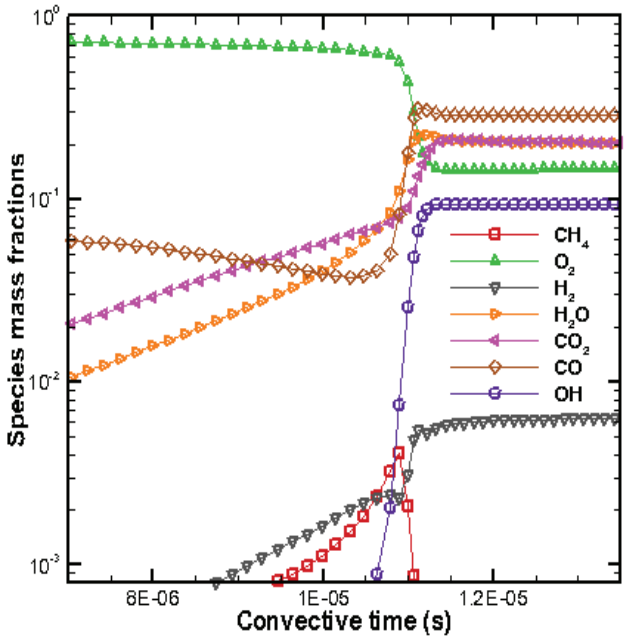

Figure 5.20. Graph depicting peak OH value with addition of CO to the reactant mixture in quantities of 10% by volume in air

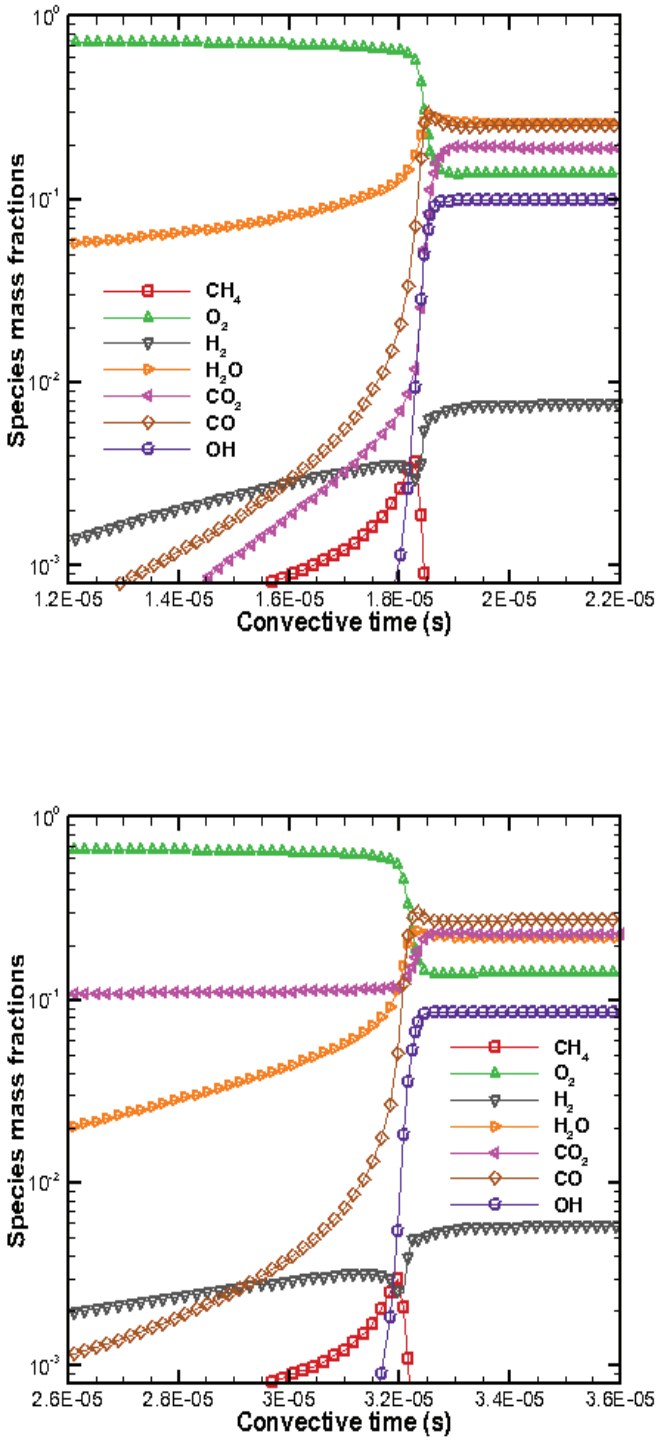

Figure 5.21. Shift in peak OH values with addition of H_2O (top) and CO_2 (bottom) to the reactant mixture in quantities of 10% by volume in air

5.2. IGNITION DELAY STUDIES

Ignition delay has a temperature dependence. As the focus of the present study was to observe the upstream temperature effects, it was of interest to observe the effect of this upstream heating on ignition delay, defined by the time taken to reach 90% of the downstream value of Y_{OH}. The case studies presented so far considered the inlet temperature to obtain the downstream characteristics of the flow and composition. In the ensuing discussion, the temperature of the upstream region in front of the shock is considered to determine the downstream characteristics. This would enable capturing the effect of radiative preheating on ignition delay characteristics.

The case studies presented in the previous section were again run with updated temperatures upstream in order to obtain the downstream flow and species profiles. Figure 5.22 shows the effects on induction times when the percentage volume of oxygen in air was varied.

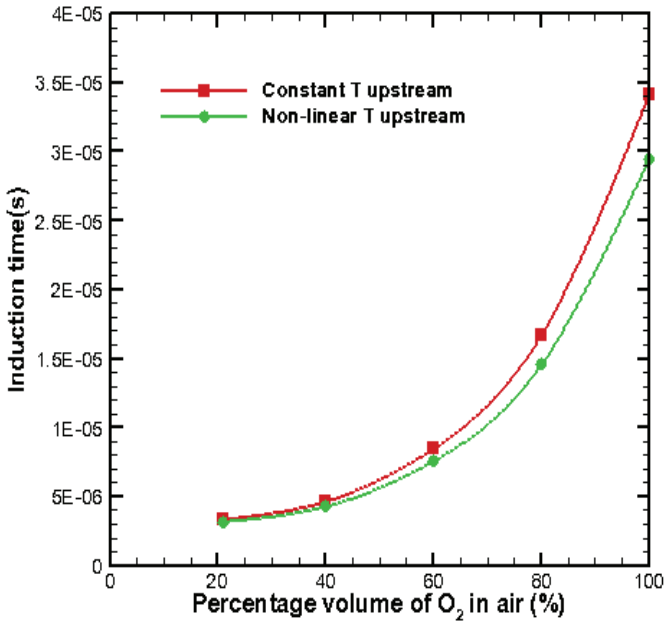

Figure 5.22. Variation in induction times when the oxygen content in air was varied

Normal levels of oxygen in air (21% by volume) showed little variation (4.86% reduction in ignition time) with radiation effects included but this effect was enhanced to 13.75% reduction in ignition delay when ethane was oxidized with only oxygen present in the air.

The gradual divergence of the curves is a natural consequence of the variation in fuel composition. The larger presence of nitrogen in air rendered the product mixture to be less sensitive to temperature changes upstream. However, as pointed out in Table 5.1., the large dependence of rate of O_2 consumption on temperature, results in the variation in upstream temperature having a noticeable impact on the induction time of the reaction. This shift in the times taken for completion of the reaction can be observed from the graphs shown below (Figure 5.23.).

When variation in induction times after incorporating radiation effects was studied for the case studies that examined the effects of inlet pressure, the percentage decrease in time dropped from a 6.02% decrease at 0.5 atm to 3.68% decrease at 1.2 atm (Figure 5.24). Evidently, increasing pressure had a very small effect on the reactions after the incorporation of the radiation model. The reason for this could be attributed to the fact that the pressure-dependent reactions (Table 5.2.) have a greater limitation on the rate of the reaction than temperature. As a result, a modification in the upstream temperature had little effect on the downstream flow.

Similar studies were carried out on the effect of radiation models on reactant mixtures diluted with CO_2 and H_2O. Ignition delay times for carbon dioxide were reduced from 14.32% at 10% dilution to 13.72% at 40% dilution. The values for water vapor dilution at corresponding levels were 13.34% and 10.78% (see Figure 5.25). Greater reductions in CO_2 induction times is due to the fact that the reaction rates are slower and any variation in temperature upstream and consequently downstream has a larger effect on the combustion times. Contrastingly, reactions for H_2O vapor dilution are much faster than CO_2 dilutions of similar magnitude. As a result, the addition of a little more energy has less impact as the reactions need less energy to proceed initially.

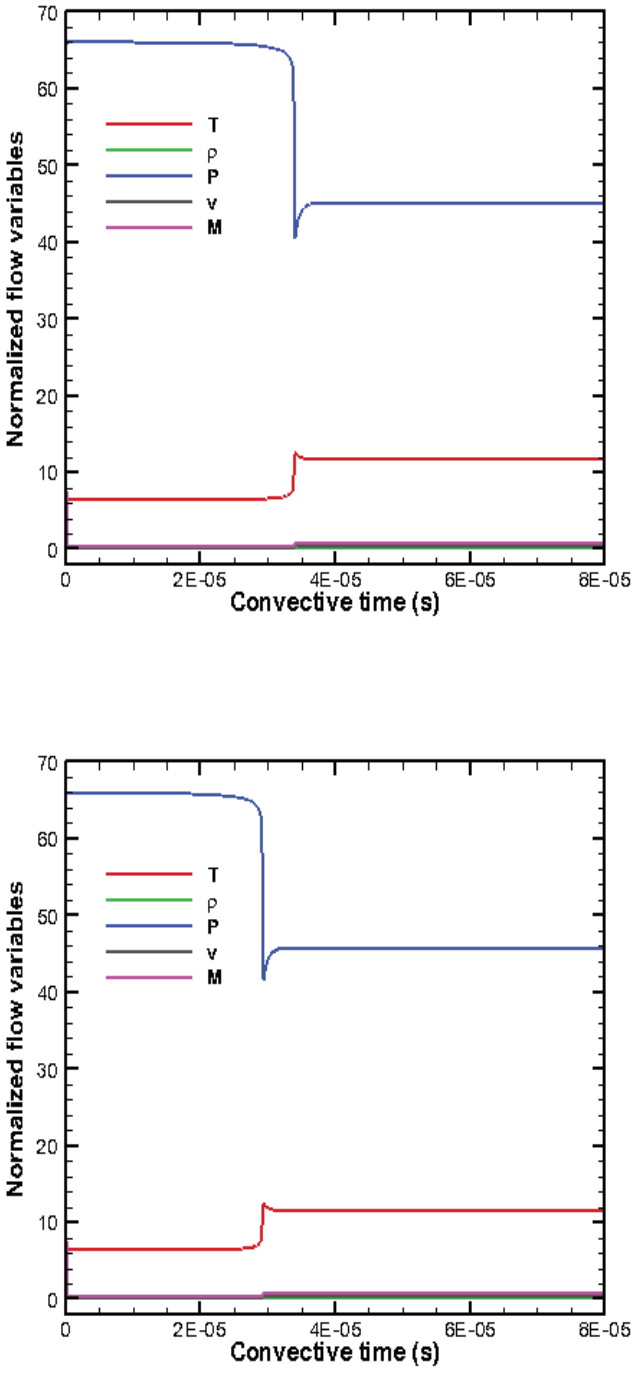

Figure 5.23. Shift in the flow variables curves from a constant temperature consideration upstream (top) to a non-linear one (bottom) for Case B

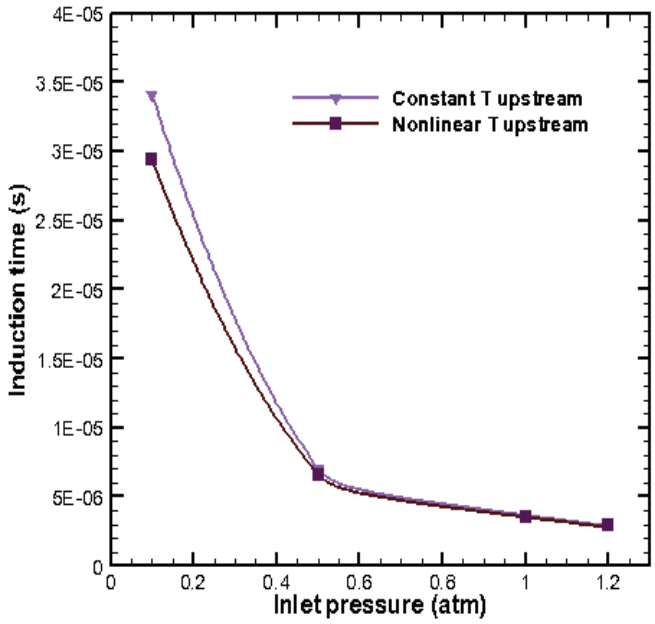

Figure 5.24. Variation in induction times when the inlet pressure was varied

The induction time curves indicate the dependence of upstream variation in temperature due to radiative heating on the activation energy of the reactions. The exponential dependence on temperature is exhibited, with higher temperatures improving the combustion times. The variations also demonstrated that a consistency in results was obtained by considering radiative pre-heating of reactants, but, the reactions themselves were more dependent on fuel composition and initial inlet temperature and pressure.

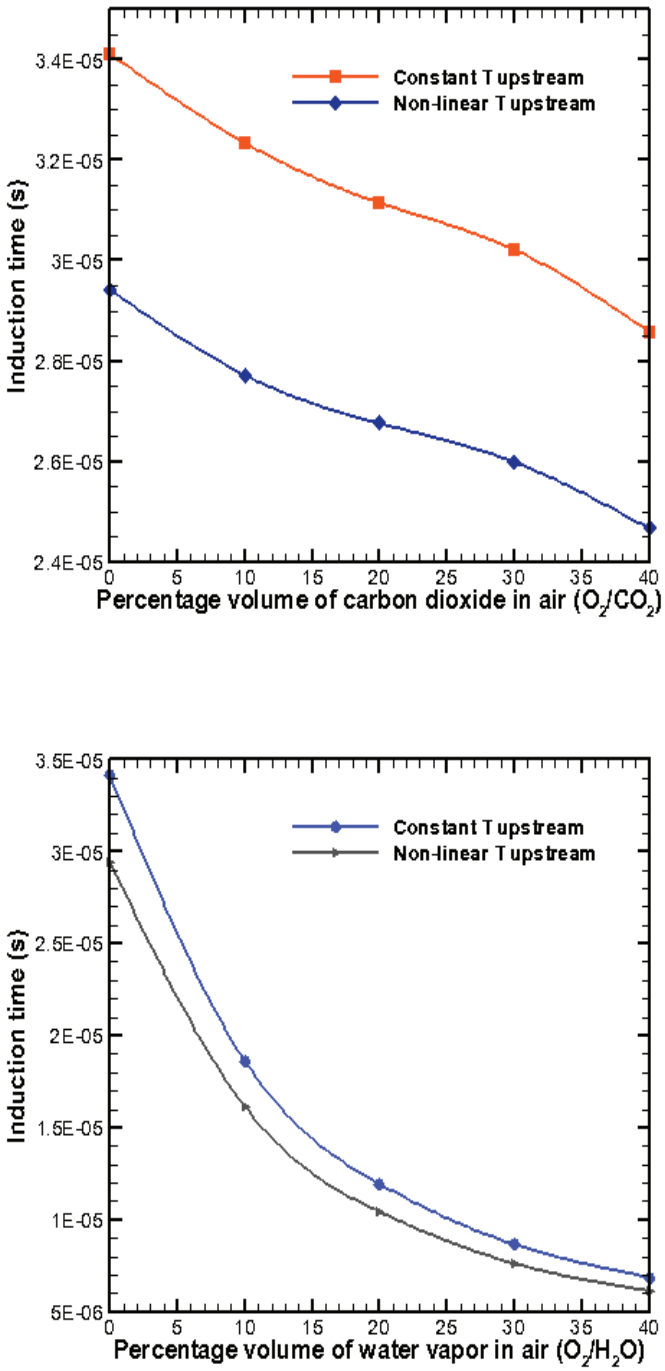

Figure 5.25. Variation in induction times when the upstream oxidizer was diluted with CO_2 (top) and H_2O (bottom)

6. CONCLUSIONS

Detonations provide a significant advantage in the raising of temperature of the reactants prior to combustion over mere adiabatic heating. The analysis of detonations in combustors would invariably require the analysis of deflagration coupled with shock waves. The present study looked at detonations in one-dimensional form in combustors. With regard to the shock wave, the assumption of constant flow properties upstream of it is quite common. The present study explored the consideration of the actual non-linear behavior of flow variables, temperature in particular, in the upstream region.

This rise in temperature which can occur from several sources was studied from the context of radiative heat transfer alone. The radiative heat transfer concentrated upon was restricted to gaseous radiative heat transfer across the shock and was simplified to a large extent by using gray gas assumption. It was believed that considerations of spectral and solid angle variations would be required for a more refined analysis especially one that focused on spectrally limited radiation and multi-dimensional physical domains. The present study was able to achieve a quantification, which is limited in literature, and a basic understanding of the phenomenon by assuming the gases to be gray.

Ethane was used as the fuel gas with air to form the reactants. The radiative transfer between the products and the reactants was assumed to occur by considering the two to be in radiative equilibrium. Weighted sum of gray gases model was used to quantify the emissivity of the products of combustion. The advantage of using such a model lay in modeling the real emissivity of the gaseous mixture which depends upon frequency in terms of a series of gray gases. They effectively translate the real gas emissivity to gray gas emissivity. The absorptivity of the reactants was quantified by optical data that deduce the absorptivity/ transmissivity of a gas sample by using Beer-Lambert's law.

In retrospect, the analysis was limited here by the dearth of sufficient and relevant experimental data and required the occasional use of the models outside their recommended ranges for certain case studies undertaken here.

Three sets of case studies were performed to understand the effect of variation of inlet conditions and upstream heating on downstream flow properties and concentrations of species. The cases studies concentrated on studying the effect of varying the composition of standard air by varying the oxygen and nitrogen levels, the effect of inlet pressure and the effect of diluting the reactant mixture with gases such as carbon-dioxide and water vapor, the products of combustion, on upstream heating. Increasing oxygen concentrations in the reactant mixture increased the induction times and decreased the absorption lengths upstream of the flow. Increased pressures had a tremendous effect on the upstream temperature behavior under the ranges studied. It was concluded that higher pressures reduced the temperature rise and absorption lengths to quite insignificant amounts. Dilution with non-hydrocarbon gases yielded interesting results in terms of absorption lengths. The absorption length could be reduced by increasing the concentration of such polyatomic gases, an aspect of interest for practical applications of the model. The effect on ignition delay due to the rise in upstream temperature was also studied for all the above cases, and reductions in induction times were observed.

The various case-studies undertaken provide for a better understanding of the entire process and more importantly supply numbers with respect to an actual hydrocarbon-gas fuel mixture; this lucid quantification was missing in the earlier models produced in the 1960's such as those by Heaslet and Baldwin [6]. The earlier models which were largely analytical in nature provided an understanding of the process. The numerical computations undertaken in the present study provide for easy incorporation in larger combustion models and are also amenable for easy verification of parametric variation of the inlet fuel-mixture.

APPENDIX A

GRAPHS INVOLVING RADIATIVE HEAT FLUX: MATLAB SOURCE CODE

```
% ------------------------------------------------------------------------
% Program to find out the range of values of radiative heat flux per
% unit mass of the fluid that can yield considerable rise in upstream
% temperature
%
%                       Pratibha Raghunandan, 2012
% ------------------------------------------------------------------------
clear all;
clc;
close all;
sigma = 5.67*10^-8;  % Stefan-Boltzmann constant
alpha = 0.1:0.1:0.6; % Absorptivity of reactant mixture
gam = 1.4;

% Input conditions
P = 0.1:0.1:2;
P1 = P*101325;  %atm to Pa
M1 = 1.5:0.1:8.0;
T1 = 300; %in K
R = 396;
%
u1 = M1*sqrt(gam*R*T1);
Tf = 2500:500:4000;
rho1 = P1/(R*T1);
Cp = 1386;
%
for(a=1:numel(alpha))
    for(b=1:numel(Tf))
        for(c=1:numel(P1))
            for(d=1:numel(M1))
                qradpum =
sigma*alpha(a)*R*T1*(Tf(b))^4/(P1(c)*M1(d)*sqrt(gam*R*T1)*Cp);
            end
        end
    end
end
%
```

```
% Plotting data
for(l=1:1:numel(Tf))
    figure
    p11=0.1:0.1:2;
    m11 =1.825:0.325:8.0;
    [x,y]=meshgrid(p11,m11);
    for(k=1:numel(alpha))
        for(i=1:numel(p11))
            for(j=1:numel(p11))
                q11(i,j)=
sigma*alpha(k)*R*T1*(Tf(l))^4/((x(i,j)*101325)*y(i,j)*sqrt(gam*R*T1)*Cp
);
            end
        end
        z11=griddata(p11,m11,q11,x,y);
        mesh(p11,m11,z11);
        xlabel('Pressure(atm)');
        ylabel('Mach number');
        zlabel('Stagnation temperature rise (K)');
    hold on;
    end
hold off;
end
```

APPENDIX B

UPSTREAM VARIATION: FORTRAN SOURCE CODE

```
      SUBROUTINE INTRO
      IMPLICIT REAL*8 (A-H,O-Z)
c
c-----------------------------------------------------------------------
c ABSTRACT  -- A code package that is used to obtain the upstream
c variation of flow variables due to radiative preheating in high
c speed flows involving combustion. It is restricted to fuel mixtures
c involving hydrocarbons
c
c                           Pratibha Raghunandan
c                            Missouri S&T, 2012
c-----------------------------------------------------------------------
c
      RETURN
      END
c
      SUBROUTINE SHKVAL(XMACH1,TEMP1,TF,P1ATM,RVAL,YVAL,IWORK,WORK,
     $           FINXS,FINPR,XMAXDX,TMPBFS,BFSMCH,PRSBFS,RHO1,EPSTOT)
      IMPLICIT REAL*8 (A-H,O-Z)
      DIMENSION IWORK(3321)
      DIMENSION WORK(2113)
      DIMENSION FINXS(21),YVAL(50)
c***********************************************************************
c     Variables
c
c     Input
c     XMACH1  -- Input Mach number of fuel mixture
c     TEMP1   -- Input temperature of fuel mixture (in K)
c     TF      -- Flame temperature (in K) obtained by execution of
c                Program CJWAVE. It takes into consideration the fuel
c                mixture and input conditions.
c     P1ATM   -- Input pressure of fuel mixture (in atm)
c     RVAL    -- Upstream mixture's specific gas constant
c                (in erg/(g. K))
c     YVAL()  -- Inlet mixture mass fractions
c     IWORK   -- Array of integer internal work space, obtained by
c                calling subroutine ckinit through program CJwave
c     WORK    -- Array of real internal work space which is to be
c                obtained in the same manner as IWORK
c
```

```
c     Output
c     RHO1    -- Density at inlet (kg/m^3)
c     TMPBFS  -- Temperature (K)-----
c     BFSMCH  -- Mach number         | -- Values in front of shock
c     PRSBFS  -- Pressure (Pa)  -----
c     EPSTOT  -- Total emissivity from the flame region
c*****************************************************************
c
c     Calculation of specific heat ratio of the upstream mixture
c     assuming it to be initially at a constant temperature.
c     Evidently, an initial approximation
      CALL CKCPBS(TEMP1,YVAL,IWORK,WORK,CPBMS)
c
c     CPBMS is in CGS units (ergs/(g*K))
c     Conversion factor to SI units
      CNVFAC = 10000.0D0
      CPMIX  = CPBMS
c
c     Upstream specific heat ratio
      GAMMIX = CPMIX/(CPMIX - RVAL)
      SIGMA  = 5.67D0 * (10.0**-8)
c
c     Obtaining the value of emissivity
      CALL EMSVTY(TF,FINXS,FINPR,XMAXDX,EPSTOT)
      P1   = P1ATM * 101325.0D0
      RHO1 = P1/(RVAL * TEMP1/CNVFAC)
      VEL1 = XMACH1 * SQRT(GAMMIX*RVAL*TEMP1/CNVFAC)
c
c     Inlet stagnation temperature
      TMP01 = TEMP1 * (1+(((GAMMIX-1)/2)*(XMACH1**2)))
c
c     Temperature rise due to radiative heat flux addition per unit
c     mass
      QRDPUM = SIGMA * EPSTOT * (TF**4)/(RHO1*VEL1*CPMIX/CNVFAC)
c
c     Stagnation temperature immediately behind the shock
      TMP02 = TMP01 + QRDPUM
c

c     Mach number immediately behind the shock
c     The governing equation can be expressed as a quadratic equation
```

```
      TRATIO = TMP02/TMP01
      COEFF1 = (1 + (GAMMIX * (XMACH1**2)))/XMACH1
      COEFF2 = 1 + (((GAMMIX-1)/2) * (XMACH1**2))
      FACMUL = TRATIO * COEFF2/(COEFF1**2)
c
c     Inputs to the quartic equation transformed to a quadratic
c     equation
      A = ((GAMMIX - 1)/2) - ((GAMMIX**2)*FACMUL)
      B = 1 - 2*GAMMIX*FACMUL
      C = -FACMUL
      DISCRM = B*B - 4.0D0*A*C
c     First root
      ROOT1 = (-B + SQRT(DISCRM))/(2.0D0*A)
c     Second root
      ROOT2 = (-B - SQRT(DISCRM))/(2.0D0*A)
      IF(DISCRM.EQ.0) THEN
         WRITE (*,*) 'Roots are real and equal'
         XMACH2 = SQRT(ROOT1)
      ELSEIF(DISCRM.GT.0) THEN
            IF (ROOT1.GT.ROOT2)THEN
                IF(ROOT1.GT.0) THEN
                    XMACH2 = SQRT(ROOT1)
                ENDIF
            ELSEIF (ROOT2.GT.ROOT1)THEN
                    IF(ROOT2.GT.0) THEN
                       XMACH2 = SQRT(ROOT2)
                    ENDIF
            ELSE
                 GOTO 10
            ENDIF
      ELSE
10        WRITE (*,*)'Roots are either negative or
     $               imaginary...Solution not practical'
          GOTO 20
      ENDIF
c
c     Temperature in front of shock
      TMPBFS = TMP02/(1+(((GAMMIX-1)/2)*(XMACH2**2)))
c
c     Storage variable for Mach number in front of shock
      BFSMCH = XMACH2
```

```
c     Pressure in front of shock
      PRSBFS = (P1*XMACH1/XMACH2)*sqrt(TMPBFS/TEMP1)
c
20    RETURN
      END
c*****************************END OF SUBROUTINE*********************
c
c
      SUBROUTINE EMSVTY(TF,FINXS,FINPR,XMAXDX,EPSTOT)
      IMPLICIT REAL*8 (A-H,O-Z)
      INTEGER    KVAL
      DIMENSION  CFK(4), ALPHA(4), BETA(4), EPS(4), FINXS(21)
      DIMENSION  IWORK(3321)
      DIMENSION  WORK(2113)
c
c*********************************************************************
c     Input
c     TF      -- Flame temperature (K)
c     FINXS   -- Array containing the final mole fractions of all
c                species
c                at the end of combustion
c     FINPR   -- Equilibrium pressure at the end of combustion (atm)
c     XMAXDX  -- The length of the combustor at the end of combustion
c                and attainment of equilibrium (m)
c
c     Output
c     EPSTOT  -- Total emissivity of the products of combustion
c
c     EMSVTY calculates the the emissivity of the products downstream
c     of the shock utilizing the emissivity model put forth by
c     Coppalle et al. This model is applicable only if TF > 2000 K
c
c     Ref:Coppalle, A.,Vervisch, P., "The Total Emissivities of High-
c         Temperature Flames," Combustion and Flame, Vol. 49, 1983,
c         pp.101-103
c*********************************************************************
c
      XMAXDX  = XMAXDX * 0.01D0   ! Conversion to m
c     File indicating the position of water and carbon dioxide in
c     kinetics species file which is input to run CHEMKIN
      OPEN (2, FILE = 'inppos.dat', FORM = 'FORMATTED',STATUS =
```

```
     $      'OLD', ACTION='READ')
c     Input for water
      READ (2,*) I1
c     Input for carbon dioxide
      READ (2,*) I2
c
c     Partial pressures of primary products of combustion (H2O and
c     CO2)
      PPWAT = FINXS(I1)*FINPR
      PPCDX = FINXS(I2)*FINPR
c
      KVAL  = PPWAT/PPCDX
c
c     Path length - pressure product
      PLPRW = PPWAT * XMAXDX
      PLPRC = PPCDX * XMAXDX
c
      CFK(1) = 0    ! Clear gas weighting factor
      ALPHA(1) = 0
      BETA(1) = 0
c     A modification to account for less than perfect values of '1'
c     and '2' for KVAL as put forth by Coppalle et al.
      IF(KVAL.LE.1)THEN
c           Coefficients
c          ------------------------
           CFK(2) = 0.464D0
           CFK(3) = 3.47D0
           CFK(4) = 121.6D0
c          ------------------------
        IF(TF.LT.2500)THEN
           ALPHA(2) = 0.136D0
           ALPHA(3) = 0.516D0
           ALPHA(4) = 0.0517D0
c          ------------------------
           BETA(2) = 0.0000726D0
           BETA(3) = -0.000163D0
           BETA(4) = -0.0000176D0
c          ------------------------
        ELSE
           ALPHA(2) = 0.464D0
           ALPHA(3) = 0.336D0
```

```
            ALPHA(4) = 0.0245D0
C           ------------------------
            BETA(2) = -0.0000596D0
            BETA(3) = -0.0000909D0
            BETA(4) = -0.00000654D0
C           ------------------------
          ENDIF
         ELSEIF(KVAL.GE.2)THEN
C           ------------------------
            CFK(2) = 0.527D0
            CFK(3) = 3.78D0
            CFK(4) = 99.54D0
C           ------------------------
          IF(TF.LT.2500)THEN
            ALPHA(2) = 0.132D0
            ALPHA(3) = 0.547D0
            ALPHA(4) = 0.0489D0
C           ------------------------
            BETA(2) = 0.0000725D0
            BETA(3) = -0.000171D0
            BETA(4) = -0.0000176D0
C           ------------------------
          ELSE
            ALPHA(2) = 0.430D0
            ALPHA(3) = 0.37D0
            ALPHA(4) = 0.0184D0
C           ------------------------
            BETA(2) = -0.0000472D0
            BETA(3) = -0.000101D0
            BETA(4) = -0.00000511D0
C           ------------------------
          ENDIF
        ENDIF
C
C       Initializer
        EPSTOT = 0
C
        DO 30 J = 1,4
            EPS(J) = ((ALPHA(J))+((BETA(J))*TF))*
     $                  (1 - EXP((-CFK(J))*(PLPRW+PLPRC)))
            EPSTOT = EPS(J) + EPSTOT
```

```
30     CONTINUE
       RETURN
       END
c*************************** END OF SUBROUTINE ********************
c
c
       SUBROUTINE UPSTRM(XMACH1,TF,P1ATM,TEMP1,RVAL,YVAL,IWORK,WORK,
      $                  FINXS,FINPR,XMAXDX,NIT)
       IMPLICIT REAL*8 (A-H,O-Z)
       CHARACTER*10 FNAME1
       DIMENSION IWORK(3321)
       DIMENSION WORK(2113)
       DIMENSION X(10000),T(10000),Q(10000),XM(10000),U(10000)
       DIMENSION P(10000),GAM(10000),CV(10000),RHO(10000)
       DIMENSION PATM(10000),CONC(10000)
       DIMENSION CP(10000),QABSB(10000)
       DIMENSION FINXS(21),YVAL(50)
c
c*********************************************************************
c      All input variables for this subroutine are the same as
c      described in the above subroutines of this code package
c*********************************************************************
c
c      Absorption coefficient on the upstream side is obtained by the
c      experimental studies carried out by Olson et al. The key
c      parameters include 'a', the absorptivity, 'b' (in cm^2/mol),
c      the optical pathlength = 9.6cm for the experiment carried out
c      and 'c', the concentration (in mol.cm^-3)
c
c      Ref: Olson, D. B.,Mallard, W. G.,Gardiner Jr., W. C.,"High
c           Temperature Absorption of the 3.39um He-Ne Laser Line by
c           Small Hydrocarbons", Applied Spectroscopy, Vol. 32, No. 5,
c           1978, pp.489-493
c
c
       CNVFAC = 10000.0D0
       FNAME1 = 'ups_trend'
       OPEN (4, FILE = FNAME1, FORM = 'FORMATTED', STATUS = 'REPLACE')
       OPEN (6, FILE = 'mole_input.dat', FORM = 'FORMATTED',
      $       STATUS = 'OLD', ACTION='READ')
c      Reading the numerator and denominator values required for
```

```
c     partial pressure calculation of the hydrocarbon gas, prior to
c     combustion
c
c     Number of moles of the hydrocarbon gas
      READ (6,*) PPHCN
c     Total number of moles in the reactant mixture
      READ (6,*) TOTMOL
c     Total number of moles of water vapor in the reacant mixture
      READ (6,*) WATNUM
c     Total number of moles of carbon dioxide in the reacant mixture
      READ (6,*) CDXNUM
c
      CALL SHKVAL(XMACH1,TEMP1,TF,P1ATM,RVAL,YVAL,IWORK,WORK,FINXS,
     $               FINPR,XMAXDX,TMPBFS,BFSMCH,PRSBFS,RHO1,EPSTOT)
c     Obtaining universal gas constant
      CALL CKRP(IWORK,WORK,RU,RUC,PA)
c     Conversion to SI units
      RU = RU * (10.0D0**-7)
      SIGMA  = 5.67D0 * (10.0D0**-8)
      PL = 9.6D0 * 10.0D0**-2
      XLEN = 10.0D0**-2  ! Grid size of 1 cm
40    NIT = 0
c     Initial values
      I = 1
      X(I) = 0
      T(I) = TMPBFS
      XM(I)= BFSMCH
      P(I) = PRSBFS
      PATM(I) = PRSBFS/101325.0D0
      Q(I) = SIGMA * EPSTOT * (TF**4)
      CALL CKCPBS(TMPBFS,YVAL,IWORK,WORK,CPBMS)
      CP(I)  = CPBMS
      GAM(I) = CP(I)/(CP(I) - RVAL)
      CP(I)  = CP(I)/CNVFAC
      RHO(I) = P(I)/(RVAL*T(I)/CNVFAC)
      U(I) = XM(I) * SQRT(GAM(I)*RVAL*T(I)/CNVFAC)
c
c     Continuity term, a constant
      D = RHO(I) * U(I)
      ABSTOL = 100
      DO WHILE(ABSTOL.GE.10.0D0**-1)
```

```
          I = I+1
          NIT = NIT+1
          IF (NIT. GE.9999)GO TO 110
          X(I) = -(I-1) * XLEN
c         Temperature based absorptivity converted to m^2/mol units
          ABSVTY = ((4.81*(10.0D0**4))-(10.01D0*T(I-1))-
     $              (0.0017D0*(T(I-1))**2))*(10.0D0**-4)
c         As absorptivity is often dependent on the partial pressure
c         of the HC gas
          FACTOR = PPHCN/TOTMOL
          CONC(I)= P(I-1)*FACTOR/(RU*T(I-1))
c
c         Absorption coefficient obtained from Beer-Lambert's Law and
c         reduced to a path length of 1 cm from Olson's model
          ABSCOF = ((ABSVTY*CONC(I)*PL)/(PL*(10.0D0**2)))*1.0D0
c
c
*****************************************************************
c         If water vapor is used in the reactant mixture, the ABSCOF
c         changes
c
          IF(WATNUM.NE.0) THEN
c            Ref: Kucerovsky, Z., and Brannen, E.,"Attenuation of 33-
c                 um laser radiation by atmospheric water vapor,"
c                 Applied Optics, Vol.15, No.9, 1976, pp. 2027-2028.
c
             EXCWAT = 1.548  ! in /Torr/m
c            Conversion to /atm/cm
             EXCWAT = 1.548/(10.0D0**2/760.0D0)
c            The extinction coefficient expressed in terms of local
c            partial pressure of water vapor and desired grid size (1
c            cm)
             EXCWAT = EXCWAT*(PATM(I-1)*WATNUM/TOTMOL)*1.0D0
             ABSCOF = ABSCOF + EXCWAT
          ENDIF
c
*****************************************************************
c         Similarly, if carbon dioxide is used in the reactant
c         mixture, the ABSCOF changes again
c
```

```
      IF(CDXNUM.NE.0) THEN
c        Ref: Schneider, C., W., Kucerovsky, Z., and Brannen, E.,
c             "Carbon dioxide absorption of He-Ne laser radiation
c              at 4.2 um: characteristics of self and nitrogen
c              broadened cases," Applied Optics, Vol.28, No.5,
c              1989, pp. 959-966.
c
         EXCCDX = 0.084  ! in /cm/atm
c        The absorption coefficient expressed in terms of local
c        partial pressure of carbon dioxide and desired grid size
c        (1 cm)
         EXCCDX = EXCCDX*(PATM(I-1)*CDXNUM/TOTMOL)*1.0D0
         ABSCOF = ABSCOF + EXCCDX
      ENDIF
c
*****************************************************************
c
      QABSB(I-1)= ABSCOF*Q(I-1)
c
c     Heat absorbed is equal to rise in enthalpy
      T(I) = T(I-1) - (QABSB(I-1)/(D*CP(I-1)))
      Q(I) = Q(I-1) - QABSB(I-1)
c
c     Obtaining Mach number
      CALL CKCPBS(T(I),YVAL,IWORK,WORK,CPBMS)
      CP(I)  = CPBMS
      GAM(I) = CP(I)/(CP(I) - RVAL)
      CP(I)  = CP(I)/CNVFAC
      A = GAM(I)
      B = -(SQRT(T(I-1)/T(I))*(1+(GAM(I-1)*(XM(I-1))**2))/XM(I-1))
      C = 1
      DISCRM = B*B - 4.0D0*A*C
c     First root
      ROOT1 = (-B + SQRT(DISCRM))/(2.0D0*A)
c     Second root
      ROOT2 = (-B - SQRT(DISCRM))/(2.0D0*A)
      IF (ROOT1.GT.BFSMCH)THEN
          XM(I) = ROOT1
      ELSE
          XM(I) = ROOT2
      ENDIF
```

```
            U(I) = XM(I) * SQRT(GAM(I)*RVAL*T(I)/CNVFAC)
c           From continuity
            RHO(I) = RHO(I-1) * U(I-1)/U(I)
c           From gas equation
            P(I) = RHO(I) * RVAL * T(I)/CNVFAC
            PATM(I) = P(I)/101325
            ABSTOL = ABS(Q(I)-Q(I-1))
         END DO
c
c        Correction for asymptotic offsets
c        Setting thresholds
         TMPTHR = (1.0D0+(10.0D0**-3))*TEMP1
         XMHTHR = (1.0D0-(10.0D0**-3))*XMACH1
         PSITHR = (1.0D0+(10.0D0**-3))*P1ATM
c
c        Employing a prediction-correction method
         EPSERR = 10.0D0**-6
         IF((T(I)-TMPTHR).GT.EPSERR)THEN
            TMPDFT = T(I)- TMPTHR
            TMPBFS = TMPBFS - TMPDFT
            GOTO 40
         ELSEIF((TMPTHR-T(I)).GT.EPSERR)THEN
            TMPDFT = TMPTHR - T(I)
            TMPBFS = TMPBFS + TMPDFT
            GOTO 40
         ENDIF
c
         IF((XMHTHR-XM(I)).GT.EPSERR) THEN
            XMCHXS = XMHTHR - XM(I)
            BFSMCH = BFSMCH + XMCHXS
            GOTO 40
         ELSEIF((XM(I)-XMHTHR).GT.EPSERR)THEN
            XMCHXS = XM(I) - XMHTHR
            BFSMCH = BFSMCH - XMCHXS
            GOTO 40
         ENDIF
c
         IF(((PSITHR*101325.0D0)-P(I)).GT.EPSERR) THEN
            PRSDFT = P(I)- (PSITHR*101325.0D0)
            PRSBFS = PRSBFS - PRSDFT
            GOTO 40
```

```
      ELSEIF((P(I)-(PSITHR*101325.0D0)).GT.EPSERR) THEN
         PRSDFT = (PSITHR*101325.0D0) - P(I)
         PRSBFS = PRSBFS + PRSDFT
         GOTO 40
      ENDIF
c
c     Data for plotting
110   DO 60 I = 1, NIT
         WRITE (4,100) X(I), T(I), Q(I), XM(I), U(I), RHO(I), PATM(I)
60    CONTINUE
c
100   FORMAT (18(E15.8,1X))
      RETURN
      END
c*****************************END OF SUBROUTINE*********************
```

BIBLIOGRAPHY

[1] Westbrook, C. K., and Dryer, F. L., "Chemical kinetics and modeling of combustion processes," *Eighteenth Symposium (International) on Combustion*, The Combustion Institute, Vol. 18, No. 1, 1981, pp. 749-767.

[2] Kailasanath, K., "Research on Pulse Detonation Combustion Systems - A Status Report," *AIAA Paper 2009 - 631*, Jan. 2009.

[3] Roy, G. D., Frolov, S. M., Borisov, A. A., and Netzer, D. W., "Pulse detonation propulsion: challenges, current status, and future perspective," *Progress in Energy and Combustion Science*, Vol. 30, 2004, pp. 545-672.

[4] Roy, G. D., "Energy Conversion through Detonative Processes," *AIAA Paper 2003 - 6010*, Aug. 2003.

[5] Vincenti, W. G., and Kruger, C. H., "Introduction to Physical Gas Dynamics," *John Wiley and Sons*, New York, 1965.

[6] Heaslet, M. A., and Baldwin, B. S., "Predictions of the Structure of Radiation-Resisted Shock Waves," *The Physics of Fluids*, Vol. 6, No. 6, 1963, pp. 781-791.

[7] Zel'dovich, Ia. B., "Shock Waves of Large Amplitude in Air," *Soviet Physics JETP*, Vol. 5, No. 5, 1957, pp. 919-927.

[8] Pearson, W. E., "On the Direct Solution of the Governing Equation for Radiation-Resisted Shock Waves," *NASA Technical Note*, Washington, D. C., Jan. 1967.

[9] Viskanta, R., and Menguc, M. P., "Radiation Heat Transfer in Combustion Systems," *Progress in Energy and Combustion Science*, Vol. 13, 1987, pp. 97-160.

[10] Lefebvre, A. H., "Flame radiation in gas turbine combustion chambers," *International Journal of Heat and Mass Transfer*, Vol. 27, No. 9, 1984, pp. 1493-1510.

[11] Viskanta, R., "Computation of radiative transfer in combustion systems," *International Journal of Numerical Methods for Heat and Fluid Flow*, Vol. 18, No. 3/4, 2008, pp. 415-442.

[12] McGrattan, K., Floyd, J., Forney, G., Baum, H., and Hostikka, S., "Development of Combustion and Radiation models for large scale fire simulation," *Third Technical Symposium on Computer Applications in Fire Protection Engineering*, Baltimore, MD, September, 2001, pp. 14-22.

[13] Hottel, H. C., and Smith, V. C., "Radiation form non-luminous flames," *Transactions of ASME, Journal of Heat Transfer*, Vol. 57, 1942, pp. 463-470.

[14] Leckner, B., "Spectral and Total Emissivity of Water Vapor and Carbon Dioxide," *Combustion and Flame*, Vol. 19, 1972, pp. 33-48.

[15] Modak, A. T., "Radiation from Products of Combustion," *Fire Safety Journal*, Vol. 1, No. 6,1979, pp. 339-361.

[16] Lallemant, N., Sayre, A., and Weber, R., "Evaluation of Emissivity Correlations for H_2O-CO_2-N_2/Air Mixtures and Coupling with Solution Methods of the Radiative Transfer Equation," *Progress in Energy and Combustion Sciences*, Vol. 22, 1996, pp. 543-574.

[17] Lou, C., Zhou, H.-C., Yu, P.-F., and Jiang, Z.-W., "Measurements of the flame emissivity and radiative properties of particulate medium in pulverized-coal-fired boiler furnace by image processing of visible radiation," *Proceedings of the Combustion Institute*, Vol. 31, 2007, pp. 2771-2778.

[18] Liu, L. H., Zhao, L., and Li, B. X., "A concept of equivalent absorption and emission coefficients for gray analysis of radiative heat transfer," *Journal of Quantitative Spectroscopy and Radiative Transfer*, Vol. 90, 2005, pp. 253-258.

[19] Jaynes, D. N., and Beam, B. H., "Hydrocarbon Gas Absorption by a HeNe Laser Beam at a 3.39-μ Wavelength," *Applied Optics*, Vol. 8, No. 8, 1969, pp. 1741-1742.

[20] Pierson, R. H., Fletcher, A. N., and Gantz, E. S. C., "Catalog of infrared spectra for qualitative analysis of gases," *Analytical Chemistry*, Vol. 28, 1956, pp. 1218-1239.

[21] Klingbeil, A. E., Jeffries, J. B., and Hanson, R. K., "Temperature-dependent mid-IR absorption spectra of gaseous hydrocarbons," *Journal of Quantitative Spectroscopy and Radiative Transfer*, Vol. 107, 2007, pp. 407420.

[22] Klingbeil, A. E., Jeffries, J. B., and Hanson, R. K., "Temperature- and pressure-dependent absorption cross sections of gaseous hydrocarbons at 3.39 μm," *Measurement Science and Technology*, Vol. 17, 2006, pp. 1950-1957.

[23] Chou, S. I., Nagali, V., Baer, D. S., and Hanson, R. K., "Hydrocarbon measurements using diode-laser absorption near 1.65 micron," *34th AIAA Aerospace Sciences Meeting and Exhibit, AIAA Paper 96-0746*, NV, 1996.

[24] Tsuboi, T., Inomata, K., Tsunoda, Y., Isobe, A.,and Nagaya, K., "Light Absorption by Hydrocarbon Molecules at 3.392 μm of He-Ne laser," *Japanese Journal of Applied Physics*, Vol. 24, No. 1, 1985, pp. 8-13.

[25] Razani, A., "Shock Waves in Gas Dynamics," *Survey in Mathematics and its Applications*, Vol. 2, 2007, pp. 59-89.

[26] Turns, S. R., "An Introduction to Combustion: Concepts and Applications," *McGraw-Hill Inc.*, New York, 2006.

[27] Clarke, J. F., "Radiation-Resisted Shock Waves," *The Physics of Fluids*, Vol. 5, No. 11, 1963, pp. 1347-1361.

[28] Sharpe, G. J., Falle, E. G., "One-dimensional numerical simulations of idealized detonations," *Proceedings: Mathematical, Physical and Engineering Sciences*, Vol. 455, No. 1983, 1999, pp. 1203-1214.

[29] Daimon, T., Matsuo, A., "Detailed features of one-dimensional detonations," *Physics of Fluids*, Vol. 15, No. 1, 2003, pp. 112-122.

[30] Hwang, P., Fedkiw, R. P., Merriman, B., Aslam, T. D., Karagozian, A. R., Osher, S. J., "Numerical resolution of pulsating detonation waves," *Combustion Theory and Modeling*, 2000.

[31] Singh, S., Lieberman, D., and Shepherd, J. E., "Combustion Behind Shock Waves," *Paper 03F-29 Western States Section/ Combustion Institute*, Los Angeles, CA, October, 2003.

[32] Li, S. C., Varatharajan, B., and Williams, F. A., "The Chemistry of JP-10 Ignition," *AIAA paper 2001-1074*, 2001.

[33] Isaac, K. M., and Scott, T., "Ignition delay and detonation wave structure using detailed chemical kinetics models," *2nd U. S. Sections Joint Meeting of the Combustion Institute*, Oakland, CA, 2001.

[34] Zhao, J., "Report on Solving One Dimensional, Steady State Combustion Problem," University of Missouri-Rolla, Mechanical and Aerospace Engineering Department report, 1991.

[35] Griner, J., and Isaac, K. M., "Induction Time and Detonation Wave Structure of Acetylene, Ethylene and JP-10," *Proceedings of the 2002 Technical Meeting of the Central States Section of the Combustion Institute*, 2002.

[36] Spadacinni, L. J., and Colket III, M. B., "Ignition delay characteristics of methane fuels," *Progress in Energy and Combustion Science*, Vol. 20, No. 5, 1994, pp. 431-460.

[37] Zhang, Y. J., Huang, Z. H., Wei, L. J., and Niu, S. D., "Experimental and kinetic study on ignition delay times of methane/hydrogen/oxygen/nitrogen mixtures by shock tube," *Chinese Science Bulletin*, Vol. 56, No. 26, 2011, pp. 2853-2861.

[38] Vasu, S. S., Davidson, D. F., and Hanson, R. K., "Jet fuel ignition delay times: Shock tube experiments over wide conditions and surrogate model predictions," *Combustion and Flame*, Vol. 152, 2008, pp. 125-143.

[39] Petersen, E. L., Hall, J. M., Smith, S. D., de Vries, J., Amadio, A. R., and Crofton, M. W., "Ignition of Lean Methane-Based Fuel Blends at Gas Turbine Pressures," *Journal of Engineering for Gas Turbines and Power*, Vol. 129, 2007, pp. 937-944.

[40] Petersen, E. L., Kalitan, D. M., Simmons, S., Bourque, G., Curran, H. J., and Simmie, J. M., "Methane/propane oxidation at high pressures: Experimental and detailed chemical kinetic modeling," *Proceedings of the Combustion Institute*, Vol. 31, 2007, pp. 447-454.

[41] Petersen, E. L., Davidson, D. F., and Hanson, R. K., "Kinetics Modeling of Shock - Induced Ignition in Low - Dilution CH_4/O_2 Mixtures at High Pressures and Intermediate Temperatures," *Combustion and Flame*, Vol. 117, 1999, pp. 272-290.

[42] Williams, F. A., "Combustion Theory," *The Benjamin/Cummings Publishing Company, Inc.*, Menlo Park, CA, 1985.

[43] Segal, C., "Scramjet Engine - Processes and Characteristics," *Cambridge University Press*, 2009.

[44] Hindmarsh, A. C., "LSODE and LSODI, Two New Initial Value Ordinary Differential Equation Solvers," *ACM SIGNUM Newsletter*, Vol. 15, No. 4, 1980, pp.10-11.

[45] Hindmarsh, A. C., "ODEPACK: A Systematized Collection of ODE Solvers. Scientific Computing," *R.S. Stepleman, et al., eds., North Holland Publishing Co.*, New York, 1983, pp. 55-64.

[46] Hill, P., and Peterson, C., "Mechanics and Thermodynamics of Propulsion," *Addison-Wesley Publishing Company, Inc.*, Massachusetts, 1992.

[47] Kee, R. J., Miller, J. A., and Jefferson, T. H., "CHEMKIN: A General-Purpose, Problem-Independent, Transportable, Fortran Chemical Kinetics Code Package," *Sandia National Laboratories Report SAND80-8003*, 1980.

[48] Coppalle, A., and Vervisch, P., "The Total Emissivities of High-Temperature Flames," *Combustion and Flame*, Vol. 49, 1983, pp. 101-108.

[49] Hottel, H. C., and Sarofim, A. F., "Radiative Transfer," McGraw-Hill, New York, 1967.

[50] Edwards, D. K., "Molecular gas band radiation," *Advances in Heat Transfer*, Academic Press, New York, Vol. 12, 1976, pp.115-193.

[51] Olson, D. B., Mallard, W. G., and Gardiner Jr., W. C., "High Temperature Absorption of the 3.39 μm He-Ne Laser Line by Small Hydrocarbons," *Applied Spectroscopy*, Vol. 32, No. 5, 1978, pp.489-493.

[52] Drake, R. P., "Theory of radiative shocks in optically thick media," *Physics of Plasmas*, Vol. 14, No. 4, 043301, 2007.

[53] Kazakov, A., and Frenklach, M., http://www.me.berkeley.edu/drm/

[54] Frenklach, M., Wang, H., Yu, C. -L., Goldenberg, M., Bowman, C. T., Hanson, R. K., Davidson, D. F., Chang, E. J., Smith, G. P., Golden, D. M., Gardiner, W. C., and Lissianski, V., http://www.me.berkeley.edu/gri−mech/, based on, Frenklach, M., Wang, H., Goldenberg, M., Smith, G. P., Golden, D. M., Bowman, C. T., Hanson, R. K., Gardiner, W. C., and Lissianski, V., "GRI-Mech - an optimized detailed chemical reaction mechanism for methane combustion," *Technical Report GRI-95/0058, Gas Research Institute*, 1995.

[55] Glassman, I., "Combustion," *Academic Press, Inc.*, Orlando, FL, 1987.

[56] Schneider, C. W., Kucerovsky, Z., and Brannen, E., "Carbon dioxide absorption of He-Ne laser radiation at 4.2μm: characteristics of self and nitrogen broadened cases," *Applied Optics*, Vol. 28, No. 5, 1989, pp. 959-966.

[57] Kucerovsky, Z., and Brannen, E., "Attenuation of 33-μm laser radiation by atmospheric water vapor," *Applied Optics*, Vol. 15, No. 9, 1976, pp. 2027-2028.

VITA

Pratibha Raghunandan was born in Bangalore, India. She pursued her Mechanical Engineering program in R. V. College of Engineering, Bangalore. She obtained her Bachelor of Engineering degree in Mechanical Engineering from Visveswariah Technological University in July 2009. She chose to pursue her Master's in Aerospace Engineering to further her interests in the field. In August 2012, she received her Master of Science degree in Aerospace Engineering from Missouri University of Science and Technology, Rolla, Missouri, USA.